Technical Sciences

16(1)

The Technical Sciences is indexed and abstracted in BazTech (http://baztech.icm.edu.pl) and in IC Journal Master List (http://journals.indexcopernicus.com)

The Journal is also available in electronic form on the web sites
http://www.uwm.edu.pl/techsci (subpage Issues)
http://wydawnictwo.uwm.edu.pl (subpage Czytelnia)

The print edition is the primary version of the Journal

PL ISSN 1505-4675

© Copyright by Wydawnictwo UWM • Olsztyn 2013

Address
ul. Jana Heweliusza 14
10-718 Olsztyn-Kortowo, Poland
tel.: +48 89 523 36 61
fax: +48 89 523 34 38
e-mail: wydawca@uwm.edu.pl

Contents

ENERGETIC EFFICIENCY OF THE SEWAGE SLUDGE COMPOSTING PROCESS IN DEPENDENCE ON STRUCTURE OF THE ADDITIVES

Krzysztof Pilarski[1], Piotr Sołowiej[2]*

[1] Institute of Biosystems Engineering, Poznan University of Life Sciences
[2] Department of the Electrotechnic Energetics Electronics and Automatics
University of Warmia and Mazury in Olsztyn

A b s t r a c t

Significant amount of the produced sewage sludge encourages to search for the most effective methods of its utilization. One of such methods is composting of the sewage sludge with various kinds of biological origin additives supporting the process. Temperature is one of most characteristic physical quantity which can describe the process course. The phase of the composting process can be defined on the basis of the temperature. The knowledge of the additives influence on the energetic efficiency of the process can help to optimize the course of composting and control it by delivering or receiving the energy surplus.

Introduction

The sewage sludge utilization is the issue arousing controversy in terms of the environmental protection and economic aspects. Sediments from municipal and rural wastewater, from agri-food industry are the rich source of nutrients for plants and have very effective soil-forming impact. The soil-forming properties of the sediments are mainly related to the presence of large amounts sediment organic matter, determining rich environment for microorganisms activities and the substances susceptible to the humus formation.

Composting of the sewage sludge as a method of its disposal has been known for a long time. Due to the physico-chemical composition of the sewage

---

[*] Corespondence: Piotr Sołowiej, Katedra Elektrotechniki, Energetyki, Elektroniki i Automatyki, Uniwersytet Warmińsko-Mazurski, ul. Oczapowskiego 11, 10-736 Olsztyn, e-mail: pit@uwm.edu.pl

sludge which is not able to ensure the proper run of the composting process, it should be supplemented with additional missing substrates. Both the additives and aeration degree have an essential importance for the amount of generated thermal energy, which is one of the main indicators certifying the accuracy and intensity of the composting process (DACH et al. 2007, SOŁOWIEJ et al. 2010a, SOŁOWIEJ et al. 2010b).

The amount of energy produced in the first phase of composting process under defined conditions can be partially (with no influence on the process quality) used as a source of thermal energy (SOŁOWIEJ 2007). Linking the amount of emitted energy with the aeration intensity, CO_2 emission and applied additives allowed to reach better efficiency of the sewage sludge composting process. This efficiency concerned the reduction of composting period, selection of the appropriate proportions of the selected additives, and the control of the entire process by the aeration regulation and used percentage of the sewage sludge dry mass in the composition of the mixture.

Description of the experiment

The aim of the study was to compare the composting process course with a special regard of the amount of generated heat energy. The experiment was conducted in parallel on four identical positions and the particular bioreactors were filled with sewage sludge mixed with additives which compositions are presented in Table 1. The content of particular options was set on the basis of

Table 1

Variants compositions of the composted additives and selected properties of the components

Specification	Component	Dry mass [%]	Share [%]	Amount in d.m. [kg]	Mass [kg]
Variant K1 (75% of sewage sludge in dry mass of the mixture)	sewage sludge	16.7	75	6.00	35.93
	straw	86	5	0.44	0.51
	sawdust	87.9	20	1.60	1.82
	humidity [%]	78.99	100	8.04	38.3
Variant K2 (60% of sewage sludge in dry mass of the mixture)	sewage sludge	16.7	60	6.10	36.53
	straw	86	5	0.50	0.58
	sawdust	87.9	35	3.60	4.10
	humidity [%]	75.25	100	10.2	41.2
Variant K3 (45% of sewage sludge in dry mass of the mixture)	sewage sludge	16.7	45	6	35.93
	straw	86	5	0.6	0.70
	sawdust	87.9	50	6.7	7.57
	humidity [%]	70.02	100	13.25	44.2
Variant K4 (30% of sewage sludge in dry mass of the mixture)	sewage sludge	16.7	30	5.4	32.34
	straw	86	5	0.9	1.05
	sawdust	87.9	65	11.5	13.03
	humidity [%]	61.75	100	17.75	46.4

The research stand was equipped with a complete system measuring the bioreactor labour parameters (temperature, air flow, air humidity, control of collected condensates and effluents, concentration of selected output gases) indispensable for calculation of heat dynamics of composting process. The previous studies have proved that during the experiments the test stand ensures the course of the process similar as in the field conditions while composting with usage of tractor aerator and at the same time allows fully control the changes in the investigated material (CZEKAŁA et al. 2006, DACH et al. 2004).
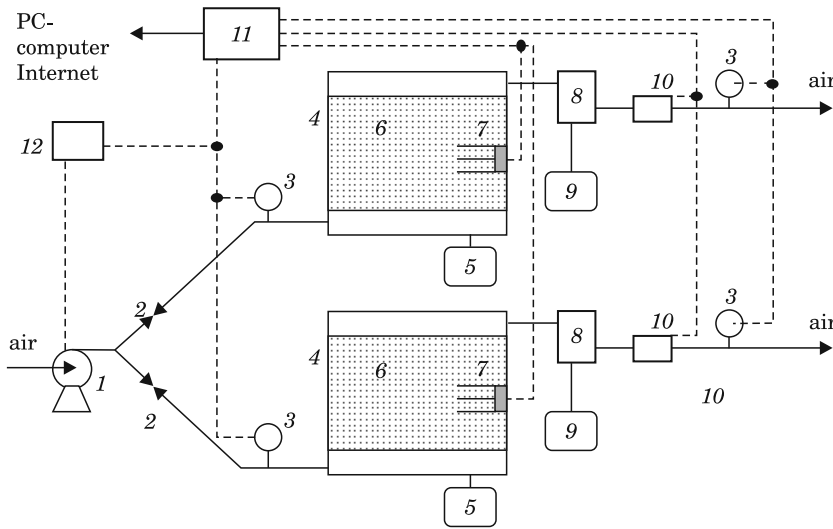
Fig. 1. Bioreactor scheme: *1* – pomp, *2* – flow controller, *3* – flow meter, *4* – insulated chamber, *5* – effluent tank, *6* – composted mass, *7* – set of temperature sensors, *8* – air cooler, *9* – condensate tank, *10* – set of gaseous sensors, *11* – recorder, *12* – pomp steering system

Methods and Results

The dynamics of the energy changes of bioreactor can be described with the overall heat balance equation:

$$\frac{dQ}{dt} = \frac{dQ_{bio}}{dt} + \frac{dQ_{intake}}{dt} - \frac{dQ_{exhaust}}{dt} - \frac{dQ_{lost}}{dt} \qquad (1)$$

where:
Q – heat contents of the bioreactor [kJ],
Q_{bio} – heat of bioreaction in composting process [kJ],

Q_{intake} – heat contained in the inlet air [kJ],
Q_{lost} – heat losses via surface of the bioreactor [kJ],
Q_{exhaust} – heat contained in the exhaust air [kJ].

In order to compare the quantity of energy produced in the composting process of the individual variants Q_{WK} was calculated as a sum of the energy in exhaust air (Q_{exhaust}) and the energy lost by walls of the bioreactor (Q_{lost}), reduced by the energy provided with intake air (Q_{intake}).

$$Q_{\text{WK}} = Q_{\text{exhaust}} + Q_{\text{strat}} - Q_{\text{intake}} \tag{2}$$

$$Q_{\text{exhaust}} = h_{\text{exhaust}} \cdot V_{\text{exhaust}} \tag{3}$$

$$Q_{\text{intake}} = h_{\text{intake}} \cdot V_{\text{intake}} \tag{4}$$

$$Q_{\text{lost}} = u \cdot t \cdot a(T_w - T_z) \tag{5}$$

where:
$h_{\text{exhaust}}, h_{\text{intake}}$ – enthalphy air streams: exhaust and intake [kJ/m^3],
$V_{\text{exhaust}}, V_{\text{intake}}$ – air volume: exhaust and intake [m^3],
u – overall heat transfer coefficient [W/m^2 K],
a – area of walls of the bioreactor [m^2],
t – time (s),
T_w – indoor temperature of the bioreactor [$^{\circ}$C],
T_z – ambient temperature [$^{\circ}$C].

In order to determine the value of enthalpy for the inlet and outlet air of the bioreactor the Kaiser method has been applied (KAISER 1996).

Using the above mentioned equation it was possible to determine the amount of energy emitted during the composting process in particular bioreactors.

The temperature is the main parameter characterizing the composting process. Figure 2 shows the temperature distribution in every variant.

The amount of carbon dioxide present in the outlet air of the bioreactor proves the activity of thermophilic organisms using oxygen in their metabolism in composting process. As it is shown in Figure 3 the amount of CO_2 leaving the bioreactor has fall down in three variants to zero in the 17th day of composting and maintained at a low level only in case of K4 variant. This certifies the end of thermophilic phase of the process.

Due to the fact that we compare only the heat energy of the process, we have taken under the consideration first 17 days of composting. In the further
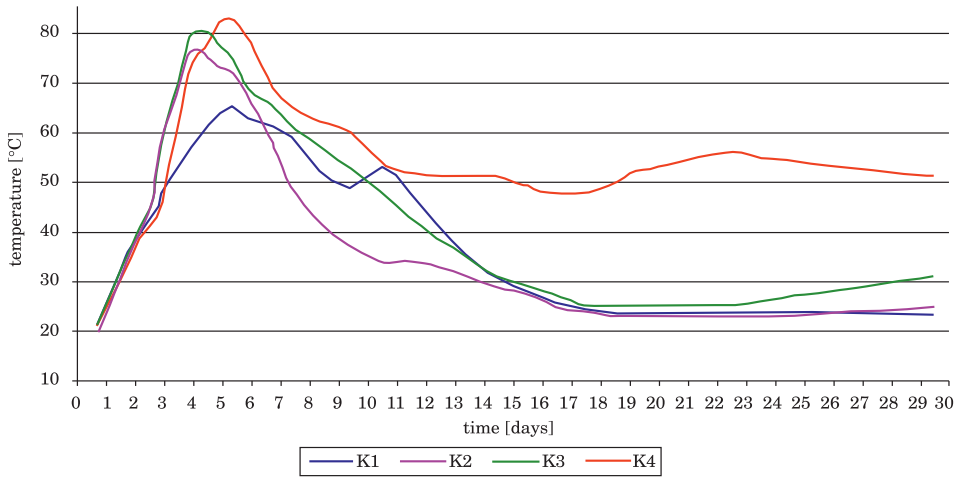
Fig. 2. Temperature distribution in particular variants
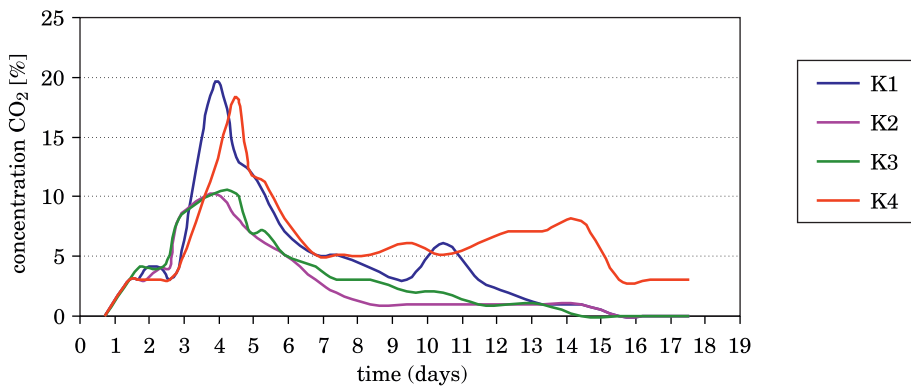
Fig. 3. Distribution of CO_2 concentration in outlet air

mesophilic part of the process apart from the heat energy also the methane is produced. Its energetic value should be taken into account in the energy balance, however it was not the subject of the research.

In consequence of conducted research the obtained data allowed to calculate the amount of energy that was emitted in composting process in particular variants (Tab. 2, Fig. 4).

Table 2

Amount of the heat emitted in particular variants in kJ for 1 kg of prepared mixture

Variant	K1	K2	K3	K4
Heat amount [kJ/kg]	1631	1342	1329	1535
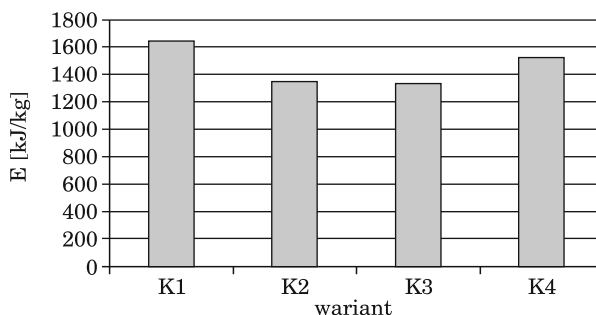
Fig. 4. Amount of the heat emitted in particular variants

Summary and the conclusions

On the basis of conducted research it has been stated that the highest temperature of composting process in the thermophilic phase is in case of K4 mixture (82ºC) and slightly lower in K2 and K3 (respectively 80 and 76ºC). Considerably lower temperature was noted in K1 mixture (65ºC). However calculation of the amount of generated heat through the respective mixtures showed that the highest amount was during composting of K1 mixture (1631 kJ/kg). The confirmation of these calculations correctness is that in K1 variant it has been stated the highest amount of produced CO_2, which proves the highest metabolic activity of thermophilic microorganisms.

Slightly lower CO_2 emission was noted in case of K4 variant and calculated energy amounted 1535 kJ/kg, the lowest were for K2 and K3, which resulted in decreased amount of produced heat – respectively 1342 kJ/kg and 1329 kJ/kg. Lower temperature – in comparison with the rest of the mixtures – noted in K1 option was caused by its higher humidity and thus allows more heat to evaporate water.

Translated by ANETA DACH

References

CZEKAŁA J., DACH J., WOLNA-MARUWKA A. 2006. *Wykorzystanie bioreaktora do badań modelowych kompostowania osadu ściekowego*. Woda – Środowisko – Obszary Wiejskie, 6, 2(18): 29–40.

DACH J., JĘDRUŚ A., KIN K., ZBYTEK Z. 2004. *Wpływ intensywności napowietrzania na przebieg procesu kompostowania obornika w bioreaktorze*. Journal of Research and Applications in Agricultural Enginering, 49(1): 40–43.

DACH J., NIŻEWSKI P., JĘDRUŚ A., BONIECKI P. 2007. *Badania wpływu aeracji na dynamikę procesu kompostowania osadów ściekowych w bioreaktorze*. Journal of Research and Applications in Agricultural Engineering, 52(1): 68–72.

KAISER J. 1995. *Modelling composting as a microbial ecosystem: a simulation approach*. Ecological Modeling, 91: 25–37.

SOŁOWIEJ P. 2007. *Przykład wykorzystania pryzmy kompostu jako niskotemperaturowego źródła ciepła*. Inżynieria Rolnicza, 8(96): 247–253.

SOŁOWIEJ P., NEUGEBAUER M., PIECHOCKI J. 2010a. *Wpływ dodatków i napowietrzania na dynamikę procesu kompostowania*. Inżynieria Rolnicza, 5(123): 259–265.

SOŁOWIEJ P., PIECHOCKI J., NEUGEBAUER M. 2010b. *Wpływ napowietrzania złoża na przebieg pierwszej fazy procesu kompostowania*. Inżynieria Rolnicza, 3(121): 193–198.

AGRICULTURAL MACHINES MAINTENANCE AND REPAIR SERVICES IN WESTERN POMERANIA

Robert Bujaczek[*1], *Kazimierz Sławiński*[1], *Andrzej Grieger*[2]

[1] Department of Agricultural Engineering, Koszalin University of Technology in Koszalin
[2] West Pomeranian University of Technology in Szczecin

A b s t r a c t

The research, determining the potential of network of maintenance workshops for agricultural machinery. A survey was conducted in 30 maintenance workshops in Western Pomerania in 2009. The study period covered the years 2007–2008, when 8,476 repairs were made. The analysed workshops have experienced staff with appropriate qualifications. 63.4% are employees with formal experience between 11 and 20 years. Employees with experience below 10 years amount 34% of staff. The demand for repair services is generated by the implementation of field work. During this period, the potential of staff and maintenance positions is fully used, while during off-season there is a significant surplus of service supply over demand. Annually, this surplus is 530% in the area of maintenance services for agricultural machinery. The effective use of the potential of the repair shops employees in the surveyed period was 30.5%.

Introduction

In agriculture, most treatments should be performed in specific agrotechnical periods. Failure to meet the basic terms of treatments, results in significantly negative effects on plant production, leading to lower yields obtained and their quality (BANASIAK 1999, KARCZMARCZYK 2005). Modern vehicles and agricultural machinery, are produced on the basis of modern design solutions and technology (JUŚCIŃSKI, PIEKARSK 2009a). As a result of natural differences in baseline characteristics of machines and their parts and external factors affecting the machine operation – it comes to frequent wear and damage that

* Corespondence: Kazimierz Sławiński, Katedra Agroinżynierii, Politechnika Koszalińska, ul. Racłwicka 15–17, 75-620 Koszalin, e-mail: agromarketing@poczta.onet.pl

must be consistently and methodically remove, and prevent their occurrence. According to the author's research (TOMCZYK 2005a,b, 2006), in the structure of the standstill of tractors and agricultural machinery from technical reasons:
– about 20% – errors in construction and manufacturing technology,
– about 25% – inadequate maintenance and storage of equipment,
– about 15% – the insufficient quality of executed repairs.

The usage of modern means of mechanization in Polish agriculture requires specialised technical background. The maintenance workshops network, currently being built with considerable support of equipment manufacturers, is highly diverse considering the quality of service. The time (needed on removing technical or technological faults occurred during their use) is the measure of reliability of machines operation systems (SKROBACKI, EKIELSKI 2006). The seasonality of works in agriculture negatively affects the use of service facilities and generates the need to study the course of developments in this market segment (JUŚCIŃSKI, PIEKARSKI 2008a,b). Taking into consideration the fact of simultaneous occurrence of many causes leading to the heterogeneity of demand, the maintenance services require many intensive logistic works (JUŚCIŃSKI, PIEKARSKI 2009b). The aim of the research was to determine the potential of network of maintenance workshops for agricultural machinery operating in Western Pomerania.

Material and Methods

The research, determining the potential of network of maintenance workshops for agricultural machinery, was conducted in months I–VI 2009 in Western Pomerania. The study period covered the years 2007–2008, when 8,476 repairs were made. In agrotechnical season (from June to November) 5,190 repairs were made, while the other repairs (3,286) were held out of this season (from December to May). The source materials were obtained by using the method of questionnaire with a closed structure. The study included 30 agricultural maintenance workshops for agricultural machinery (13 workshops, 11 workshops non-specialist, 6 authorized service). The main selection criterion of workshops was the ability to perform complex repairs (mechanical and electronic) for agricultural machinery and tractors manufactured until 2005. The sample size was chosen by using the method of purposive sampling. The sample was made more detailed according to method of selection of typical individuals. The evaluation of collected data was made using the statistical analysis of R-Spearman statistical correlation.

Results

The structure of crops in Western Pomerania is dominated by cereal crops occupying 73.0% sown area. Industrial plants amount 16.4%, fodder crops – 4.6% and potatoes – 3.6%. Such a structure of crops has an impact on farm equipment with the means of mechanization. According to the National Agricultural Census 2001 agricultural tractors were in 30.2% farms. More than 10% farms with an area of over 1 ha of agricultural land had combine harvesters, 7.5% – balers, 5.5% – potato harvesters, 1.4% – beet harvesters. The protection of agricultural measures requires broad action to guarantee the functional and time efficiency of logistic customer service (PIEKARSKI 1997).

The promptness of realization of specific agrotechnical practices plays a crucial role on a farm. These fixed dates largely depend on weather conditions. Each day of delay may expose farmers on different kind of loss, which in consequence reduce his income. Facing a machine failure, a part of farms with outdated construction equipment decide to repair it themselves. While farmers with modern machinery must have it repaired by a specialized workshop. More than a half – 57.8% of researched workshops, in order to use their full repair potential, takes a machine for repair in less than 3 days from the date of notification (Fig. 1). In 32.6 % analysed workshops the time of expectation on repair ranged from 4 to 7 days. In other service plants it takes more than 7 days.
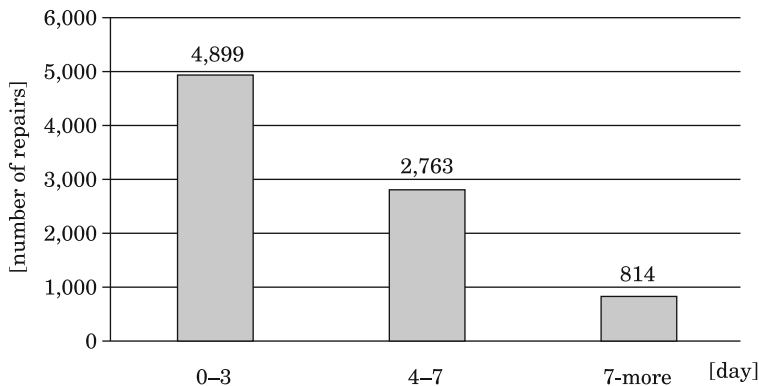

Fig. 1. The waiting time for repair

The waiting time for repair depended largely on the seasonality of field work and the number of positions serving in the workshop.

The repair time is an extremely important element in total repair (Fig. 2). Over half of repairs- 53% is made in 2 days from the moment of arrival of

a machine to workshop. Workshops make 20% of ordered repairs in a day, while the remaining 27% of repairs is made in 3 to 7 days time. The repair time of agricultural machines depends on the degree of damage. In situation when the failure of specific machine is repetitive and typical, workshops are earlier supplied with spare parts and the repair time is relatively short. When the failure is rare, workshops are not able to eliminate it earlier than in 3 days.
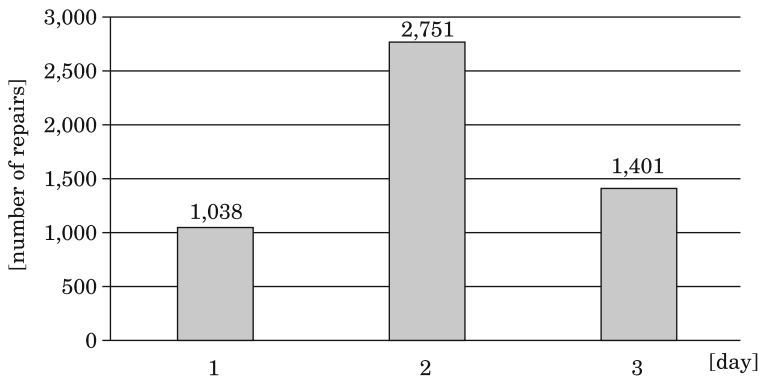
Fig. 2. The mean repair time in the season field works (months of June – November)

Repairs last longer when farm works are not being done. In 47% of cases, they may take up to 3 days. 41% of repairs is made in time from 4 to 7 days, and the remaining 12% of failures is eliminated in more than 7 days. The longer repair time during field work off-season results from the fact that the machines that are used seasonally are taken for major repairs. During field work season there are also the repairs of machines which at this time are rarely used. The extension of repair time also results from the fact that workshops are supplied with less spare parts.

The analysed workshops have experienced staff with appropriate qualifications. 63.4% are employees with formal experience between 11 and 20 years. Employees with experience below 10 years amount 34% of staff.

The demand for repair services is generated by the realization of agricultural measures at harvesting of cereals, oilseeds and root crops (KARCZMARCZYK 2005, BANASIAK 1999). During this period, the potential of staff and maintenance positions is fully used, while during off-season there is a significant surplus of service supply over demand. Annually, this surplus is 530% in the area of maintenance services for agricultural machinery The number of hours of effective work in relation to potential of employees in the surveyed workshops was 30.5% (Fig. 4).
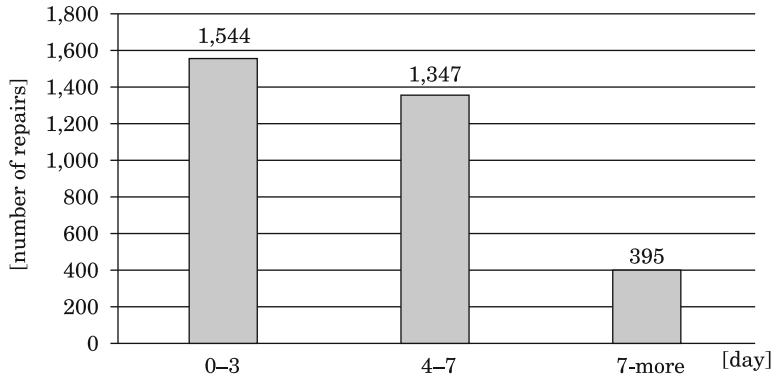
Fig. 3. The mean repair time the off-season field works (months December – May)
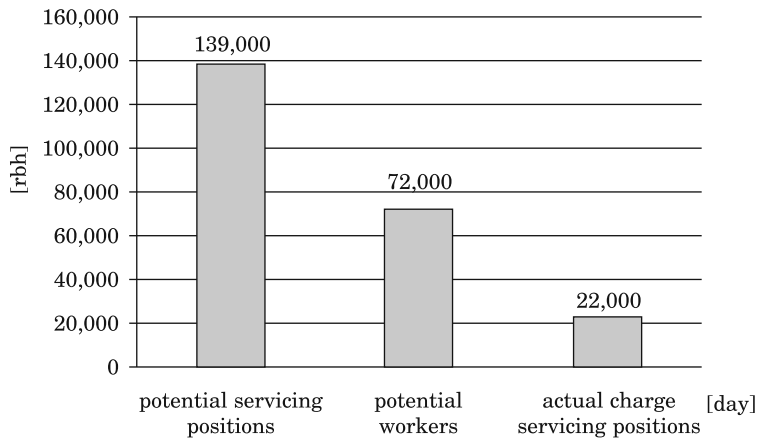
Fig. 4. Use of repair stations per year

Conclusion

The purchasers of agricultural equipment have increasing demands about the quality of repairs. The breakdowns of agricultural machines often interrupt the technological process. The time of machine repair during intensive works in farm is a crucial element in the quality of their realization.

Qualitative changes in the construction of agricultural machinery caused the necessity to adjust the size of technical background to their service.

There is a significant surplus (530%) of supply over demand in the area of maintenance services for agricultural machinery (especially in the area of service).

The effective use of the potential of employees in the surveyed maintenance workshops stands at 30.5%.

The level of execution of the routine technical maintenance and repairs is one of the most important factors having the essential influence on the process of machines, tractors and agricultural transport means wear. The factors which have a decisive influence on the technical maintenance and repairs are design solutions of individual items of machines, the workshops equipment of technical facilities with modern tools and devices, as well as the technical level and the qualifications of repair staff (TOMCZYK 2010).

Translated by AUTHORS

References

Agrotechnika roślin uprawnych. 2005. Red. S. Karczmarczyk. Wyd. Akademii Rolniczej w Szczecinie.

Agrotechnologia. 1999. Red. J. Banasiak. Wyd. Naukowe PWN, Warszawa – Wrocław.

JUŚCIŃSKI S., PIEKARSKI W. 2008a. *Systemy logistyczne w procesie zarządzania dystrybucją ciągników i maszyn rolniczych*. Acta Agrophisica, 12(1): 113–124.

JUŚCIŃSKI S., PIEKARSKI W. 2008b. *Analiza statystyczna obsługi serwisowej ciągników rolniczych w aspekcie odległości od siedziby firmy*. Inżynieria Rolnicza, 2(100): 57–65.

JUŚCIŃSKI S., PIEKARSKI W. 2009a. *Naprawy pogwarancyjne ciągników rolniczych jako element autoryzowanego systemu dystrybucji*. Inżynieria Rolnicza, 8(117): 23–30.

JUŚCIŃSKI S., PIEKARSKI W. 2009b. *Rozkład zapotrzebowania na przeglądy serwisowe ciągników rolniczych w aspekcie terminów agrotechnicznych*. Inżynieria Rolnicza, 8(117): 31–38.

PIEKARSKI W. 1997. *Analiza oddziaływania agregatów ciągnikowych na środowisko przyrodnicze*. Wyd. Akademia Rolnicza, Lublin.

SKROBACKI A., EKIELSKI A. 2006. *Pojazdy i ciągniki rolnicze*. Wyd. Wieś Jutra, Warszawa.

TOMCZYK W. 2005a. *Uwarunkowania racjonalnego procesu użytkowania maszyn i urządzeń rolniczych*. Inżynieria Rolnicza, 7: 359–366.

TOMCZYK W. 2005b. *Aspekty ekologii w konstruowaniu i odnowie maszyn i urządzeń*. Journal of Research and Applications in Agricultural Engineering, 4: 45–47.

TOMCZYK W. 2006. *Problem jakości w procesie eksploatacji i odnowy maszyn i urządzeń*. Problemy Jakości, 10: 50–52.

TOMCZYK W. 2010. *Metoda technologiczności odnowy maszyn rolniczych*. Inżynieria Rolnicza, 4(122): 261–267.

ANALYSIS OF HEIGHT DETERMINATION USING THE ASG-EUPOS NAWGEO SERVICE

Karol Dawidowicz[*]

Institute of Geodesy
University of Warmia and Mazury in Olsztyn

A b s t r a c t

GNSS observations carried out in a network of permanent stations are a complex systems which offer post-processing as well as corrections sent in real-time and the creation of so-called virtual observations. Currently, there are several Network-based Real Time Kinematic (NRTK) services around the world. In Poland, such a system has been in operation since June 2008, known as the Polish Active Geodetic Network (ASG-EUPOS). Three real-time correction services and two post-processing services are currently used by users.

NRTK technique uses GNSS observations gathered from a network of Continuously Operating Reference Stations (CORS) in order to generate more reliable error models that can mitigate the distance dependent errors within the area covered by the CORS. This method has been developed and tested considerably by many scientists during recent years. These studies have demonstrated the high centimeter accuracy that can be achieved using NRTK technique.

This study analyzed the accuracy of the height determination with NRTK measurements using ASG-EUPOS. The results obtained show that RTK ASG-EUPOS height measurements are characterized by high precision, but the normal height measurements compared to the height measurements obtained from precise leveling, probably due to some systematic errors (the mean of many measurements differs significantly from the actual value) are not so accurate. In this case, fitting NRTK results to a precise leveling network may significantly improve the results. In presented test this resulted in reducing NRTK normal height determination errors by 70 percent.

Introduction

The EUropean Position Determination System (EUPOS) project was started in 2002 in Berlin. It's purpose was to create a homogenous ground-based GNSS support system in Central and Eastern Europe. In Poland,

---
[*] Corespondence: Karol Dawidowicz, Instytut Geodezji, Uniwersytet Warmińsko-Mazurski, ul. Oczapowskiego 1, 10-719 Olsztyn, tel. 48 89 523-45-26, e-mail: karol.dawidowicz@uwm.edu.pl

ASG-EUPOS was launched in June 2008 (Bosy et al. 2007, 2008). The ASG-EUPOS network plays the role of a geodetic reference system in Poland. The connection of the ASG-EUPOS stations with the EUREF Permanent Network (EPN) stations in Poland allows the implementation of the European Terrestrial Reference System '89 (ETRS89) system in Poland. For this purpose, the system activity has to be constantly monitored and controlled.

The ASG-EUPOS is a multi-functional satellite positioning system. Its structure is divided into three basic segments: – reference stations, management and user segments. These segments working together support precise real-time positioning and post-processing applications. The reference stations network, presented on figure 1, currently (October 2012) consists of 99 Polish (81 with GPS module and 18 with GPS/GLONASS module) and 22 foreign stations.
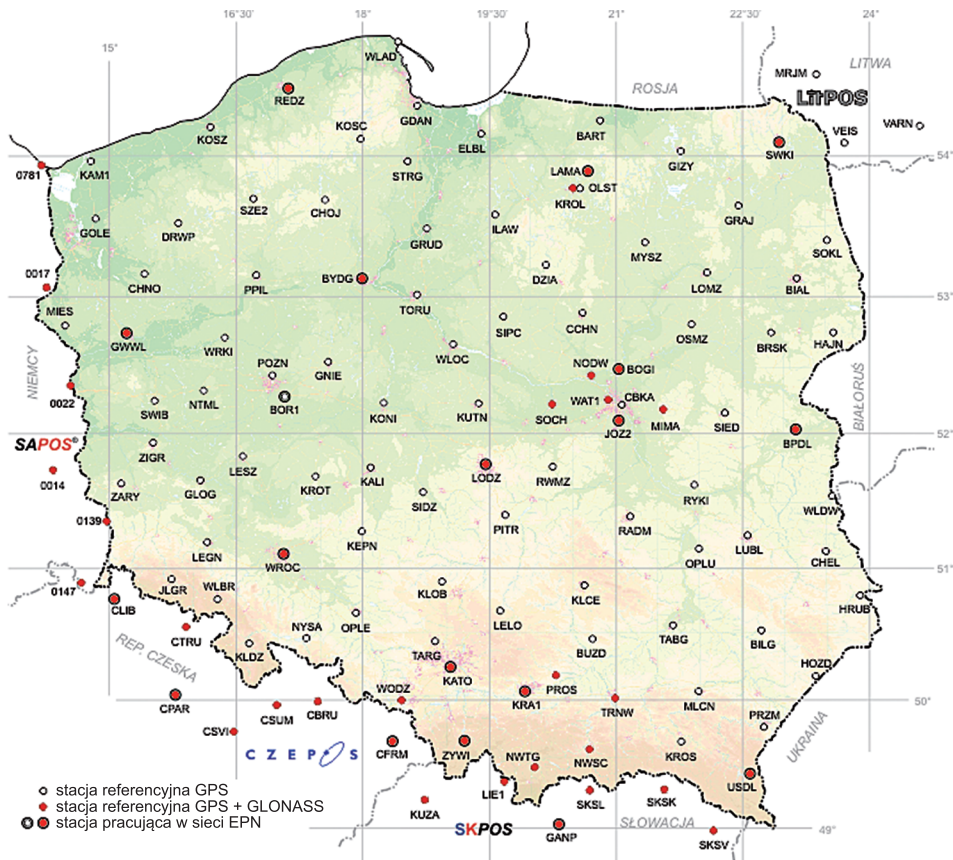

Fig. 1. ASG-EUPOS point distribution
Source: ASG-Eupos, www.asgeupos.pl (access: 12.08.2012)

The mean distance between reference stations is below 70 km. The stations are regularly distributed, creating a homogenous network which covers all of Poland. The ASG-EUPOS services enable the transfer of reference frames into real applications in the field. Three real-time correction services and two post-processing services are currently used by users. Table 1 shows the real-time services available in the ASG-EUPOS system.

Table 1

Real-time ASG-EUPOS services

Service group	Data access	Service name	Survey method	Estimated precision	Minimum hardware requirements
Real-time services	GSM/ /Internet	NAWGEO	kinematic RTK	0.03 m (horiz) 0.05 m (vert.)	L1/L2 GNSS RTK receiver, communication module
		KODGIS	kinematic DGPS	0.2 – 0.5 m	L1 DGNSS receiver, communication module
		NAWGIS		1.0 – 3.0 m	

NAWGEO is a fundamental ASG-EUPOS service which provides corrections for real-time RTK positioning. It provides high accuracy (position precision about 0.03 m) for the measurement of kinematic and static objects. Other services are targeted at users who do not require such high accuracy. Recommendations for surveying measurements using ASG-EUPOS are available, among others, in Technical guidelines G-1.12, 2008 and Technical recommendations, 2011.

In the NAWGEO service the user has the possibility to choose among various types of RTK corrections: traditional corrections from a single base station and network corrections like Master and Auxiliary Concept (MAC) and Virtual Reference Station (VRS).

Single base station RTK positioning is a technique that allows centimeter level accuracy position determination in real time through differencing similar errors and biases that are caused by atmospheric effects and GNSS satellite orbit errors (so called: distance dependent errors) and clock bias in carrier phase observations at both ends of a baseline. One significant drawback of this single base RTK approach is that the maximum distance between the reference and the rover receiver must not exceed 10 to 20 km in order to be able to rapidly and reliably resolve the carrier phase ambiguities. This limitation is caused by the above-mentioned distance-dependent biases (WANNINGER 2004, WEGNER, WANNINGER 2005).

NRTK positioning overcomes such drawbacks and can increases accuracy by accurately modeling the distance dependent errors at the rover position using measurements of an array of reference stations. In order to increase the distance from the reference station for which it is possible to achieve a cen-

timeter level solution, various methods were developed based on the use of networks of GNSS reference stations.

The essence of the VRS concept is to use real observations of several reference stations to create observations for a virtual station situated at the approximate position of the rover. This approach allows modeling of distance-dependent systematic errors a more precise than in standard RTK positioning.

The VRS technique is currently the most popular NRTK method due to the fact that it does not require modifications of the user software. The implementation of the VRS technique requires at least three reference stations which are connected to a network server, and the rover must be capable of two-way communication. The rover sends its approximate position via a wireless communication link in the NMEA format to the network processing centre where computations are carried out for each user. The processing center generates, in real time, a virtual reference station data at the initial rover position. This is done through geometrical shift of the pseudo-range and the carrier phase data from the closest reference station to the virtual location and then through adding the interpolated errors from the network error models. This generated VRS data is then sent to the user and, finally, just as if the VRS data had come from a physical reference station, the rover receiver uses standard single-baseline algorithms to determine the coordinates of the user's receiver in near-real-time kinematic or post-processed modes (EL-MOWAFY 2012, ERHU at al. 2006, WANNINGER 1997, 1999, 2002, 2003, VOLLATH et al. 2000).

The Master-Auxiliary Concept was introduced by EULER et al. (2001) and has been shown to deliver high-quality results (e.g. EULER et al. 2002, 2003). It is designed to transmit all relevant correction data from a CORS network to the rover in a highly compact form. In the MAC approach, the rover sends its approximate position to the processing centre. The centre determines for this user the appropriate master station – usually the closest reference station and identifies the auxiliary reference stations. These stations are chosen within a catch circle of a predefined radius (e.g. 70 km) around the rover, and with a pre-set number (e.g. from 3 to 7). The rover receives different types of information comprising:

  – the coordinates and raw measurements of the Master station,
  – measurement corrections at the Master station,
  – correction differences between the Master and Auxiliary stations.

After receiving the MAC information, the rover software is free to decide the method of interpolating the corrections at its location (BROWN et al. 2006, EL-MOWAFY 2012).

GNSS leveling

Satellite leveling is the procedure used to determination orthometric (normal) heights, on the basis of ellipsoidal heights derived from GNSS techniques and additional information which provide geoid (quasi-geoid) undulation determination. In the absolute approach, normal height can be derived from the equation (e.g. HOFMANN-WELLENHOF at al. 2008):

$$H = h - N \tag{1}$$

where:
H – normal height,
h – ellipsoidal height,
N – geoid undulation.

GNSS measurements performed in the ASG-EUPOS system and so-called "national" geoid models are connected with ETRS89 system thus the normal heights of points can be calculated from the above relation. Due to some systematic errors that may occur in the geoid model or in GNSS measurements, the Technical Instruction G-2 recommends an additional connection to the national vertical network. In such an approach, we talk about relative satellite leveling in which we compute normal height differences: $\Delta H = \Delta h - \Delta N$, where: $\Delta H = H_2 - H_1$, $\Delta h = h_2 - h_1$, $\Delta N = N_2 - N_1$. Knowing, for example, H_1 we can compute H_2 on the basis of measured Δh and ΔN. Such an approach can eliminates, especially on short distances, mentioned above systematic errors. Unfortunately, due to the fact that ASG-EUPOS stations mainly mounted on the roofs of buildings do not yet have accurate normal heights and because of the long distances between the stations, such an approach requires additional leveling measurements.

It is well-known that the measurements performed in real time are usually characterized by a lower accuracy than static measurements and the accuracy of height determination is less accurate than the horizontal position. Currently, the most accurate measurement technique in real-time is called RTK. One of the main limiting factors of the accuracy of RTK is the distance from the reference station (the impact of distance-dependent errors such as satellite orbits or propagation noise) and a solution for this problem was found in surface corrections. This involves the widely-accepted technique of using such corrections known as the NRTK system.

In the paper we analyze the accuracy of the height determination with NRTK measurements using ASG-EUPOS. Similar studies, using ASG-EUPOS services, aimed mainly at testing the accuracy of normal height determination

are presented in, e.g. HADAŚ, BOSY J., 2009. In other CORS analogous research have been made in e.g. APONTE et al. 2009, EDWARDS et al. 2010, MENG et al. 2007.

Several points were selected for testing. Selected points were characterized by different distance to the nearest CORS station and the level of obstacles. On points normal heights were detrmined by precise leveling and several NRTK measurement sessions using the NAWGEO service were performed. In that measurements three types of correction were used which were available in NAWGEO. Such carried test measurements allowed in different ways examine the accuracy of height determination using NAVGEO service. It has been studied e.g. impact of the distance to the nearest CORS stations, level of obstacles, type of used corrections, method of fitting to the precise leveling network.

Test measurement

For analysis two test areas, called respectively KORTOWO and TRA-VERSE, were selected (Fig. 2).
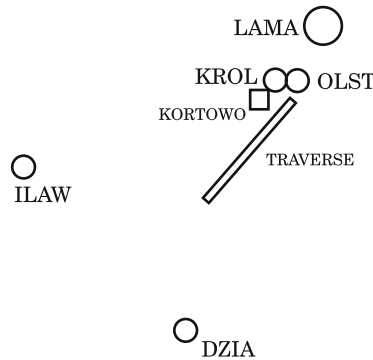
Fig. 2. Research areas and nearest ASG-EUPOS stations

The investigation in KORTOWO obiect were mainly targeted at studing the impact of level of obstacles to height determination using NAVGEO service. Two points (0001 and 0002) were marked under conditions of limited availability of satellites (nearby buildings and trees) and the remaining two points were characterized by good measurement conditions. The obstacles diagrams for KORTOWO obiect points are presented in figure 3.
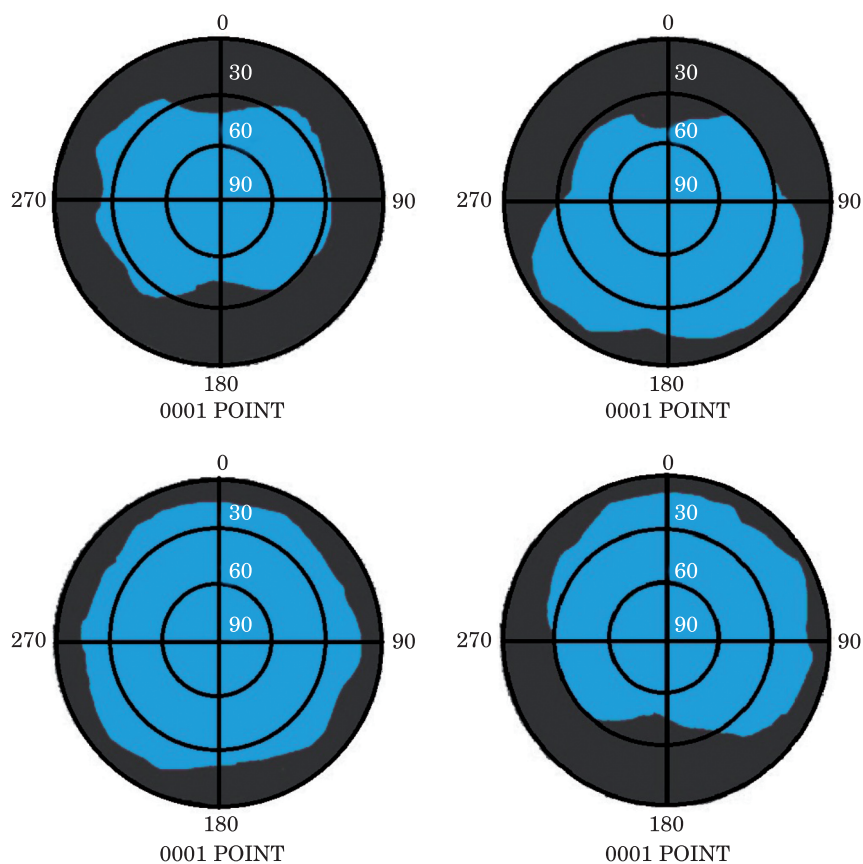
Fig. 3. The obstacles diagrams for KORTOWO points

In TRAVERSE area the main goal of the work is to show the impact of distance to the nearest ASG-EUPOS stations on NRTK heights determination. Six points were marked at different distances from OLST and KROL stations (Fig. 4).

All investigations was intended to evaluate the quality of NAWGEO service from the end users' pointof view: the corrections received using the tests were the same as any other subscribers would have received.

For selected test points, normal heights were determined by precise leveling (Tab. 2) on the basis of 2nd order benchmarks of the national leveling network. Table 2 also includes the separations between a quasi-geoid and an ellipsoid on the measured points calculated with the "QGEOID-PG" model used in the ASG-EUPOS system.
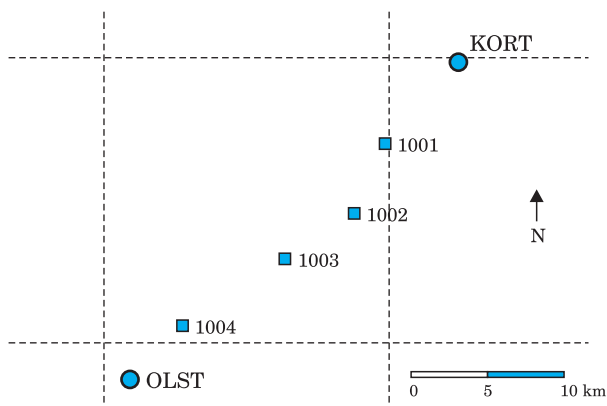
Fig. 4. TRAVERSE test area

Table 2

Normal height and quasi-geoid to ellipsoid separation on selected points

Point number	0001	0002	0003	0004	KORT	OLST
Normal height [m]	117.234	115.318	104.995	105.974	122.446	172.564
Geoid undulation [m]	29.805	29.803	29.818	29.819	29.794	30.206

A Leica Viva receiver integrated with a pole carbon fiber (with a 20^{cc} circular level) was used for measurements collection. Measurement parameters: antenna height 2.00 m; elevation angle 10°; number of RTK measurements which averaged position 5 (KORTOWO) and 15 (TRAVERSE). Position averaging mode: weighted average – an average in which position to be averaged is assigned a weight calculated using e.g. distances to CORS stations, RMS values. Sessions were made between 9:00 and 15:00 local time one by one on individual points in accordance with their numbers. The Ionosphere Index I95 RTK–VRS in each session was between normal and medium activity. Index 95 values reflect the intensity of ionospheric activity. The I95 values are computed from the ionospheric corrections for all satellites at all network station for the respective hour – the worst 5% of data are rejected. The values of the I95 have the following meaning: 2 – normal activity, 4 – medium activity, 8 – high activity.

The PDOP coefficient never exceeded 2.5. In the measurements, three types of correction were used which were available in NAWGEO: Single Stations (**SS**), Virtual Reference Stations (**VRS**), Master-Auxiliary Concept (**MAC**). The measurement session program is presented in table 3. The transition between each type of corrections take place every 10 individual measurements.

Measurement session program

Correction type	Number of NRTK measurements for each point in session				
	KORTOWO				TRAVERSE
	24 March	25 March	24 May	28 May	18 October
SS	100	100	–	–	50
VRS	100	100	100	100	50
MAC	–	–	100	100	50

All measurements were done in a field by surveyor – only fixed ambiguity solutions were recorded.

Analysis of results

Normal heights obtained from geometric precise leveling and heights obtained from RTK-NAWGEO leveling in KORTOWO area are presented in Figures 5–8. Black solid lines indicate heights obtained from precise leveling, green solid lines represent heights obtained from NRTK leveling using VRS corrections, blue – using SS corrections and red – using MAC corrections. In all approaches "real" errors were calculated as difference between the normal heights obtained from precise leveling and heights obtained from successive epochs of NRTK. Additionally for individual sessions the following information are presented in table 4: maximum height change, standard deviation, average normal height difference between geometric leveling and NRTK leveling.

From Figures 5–8 it can be seen that there are clear systematic differences between solutions using various types of correction. The biggest occurred in 24 May sessions, the smallest – in 28 May sessions. Generally it can be assumed that, except 28 May sessions where very small height differences were obtained, depending on the used type of correction heights differ up to several centimeters.

It is also a noticeable that heights obtained from NRTK measurements are significantly smaller than heights derived from geometric leveling.

For point 1 in MAC 24.05 session, at the end of the session, an unexpected jump in height in the 17 cm size occurred. The reason for this jump is unclear. This can be due to undetected cycle slip or wrong ambiguity solutions. Points measured under conditions of limited availability of satellites can usually have problems both with the visibility of satellites and the receiving of the correction message. Further investigation needs to be carried out in order to check reasons for this type of jumps.
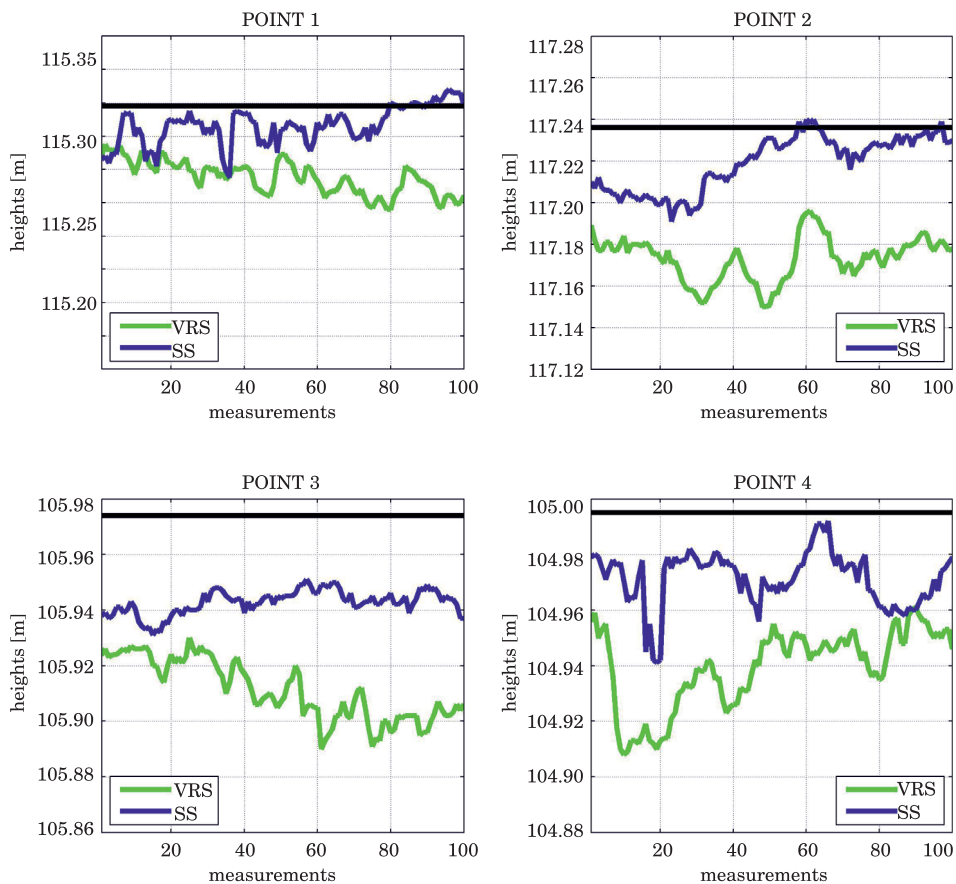
Fig. 5. Normal heights obtained from precise leveling and heights obtained from NRTK measurements in 24 March sessions
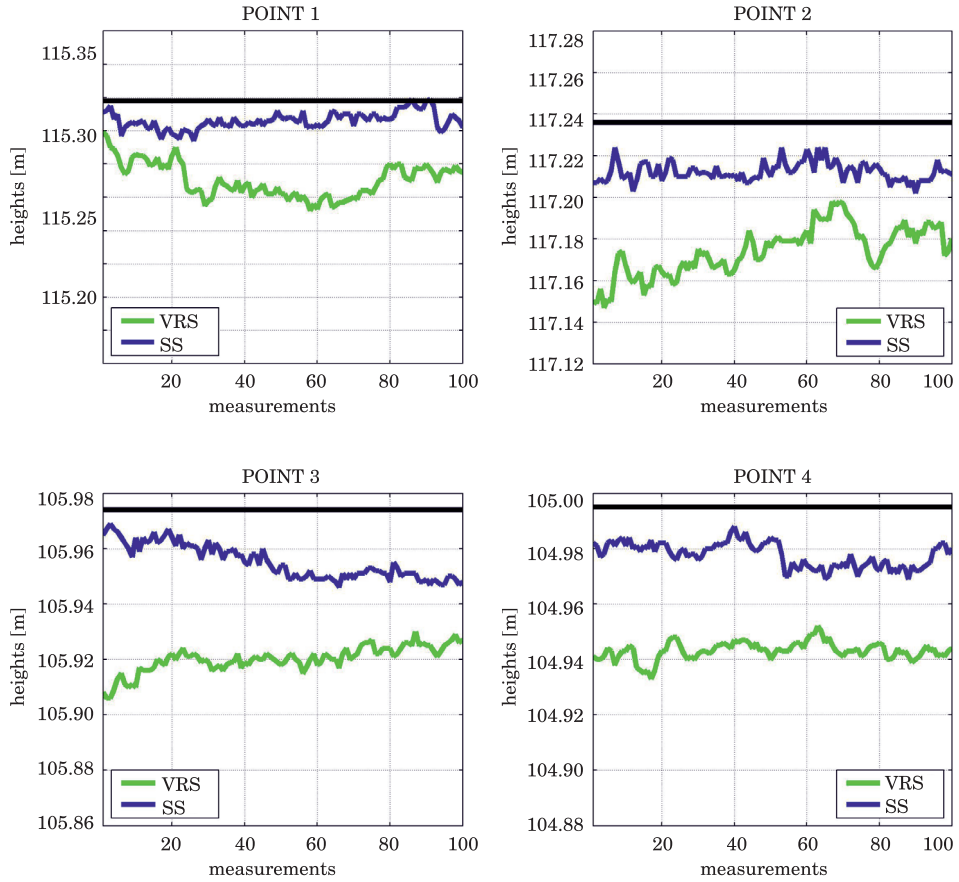
Fig. 6. Normal heights obtained from precise leveling and heights obtained from NRTK measurements in 25 March sessions
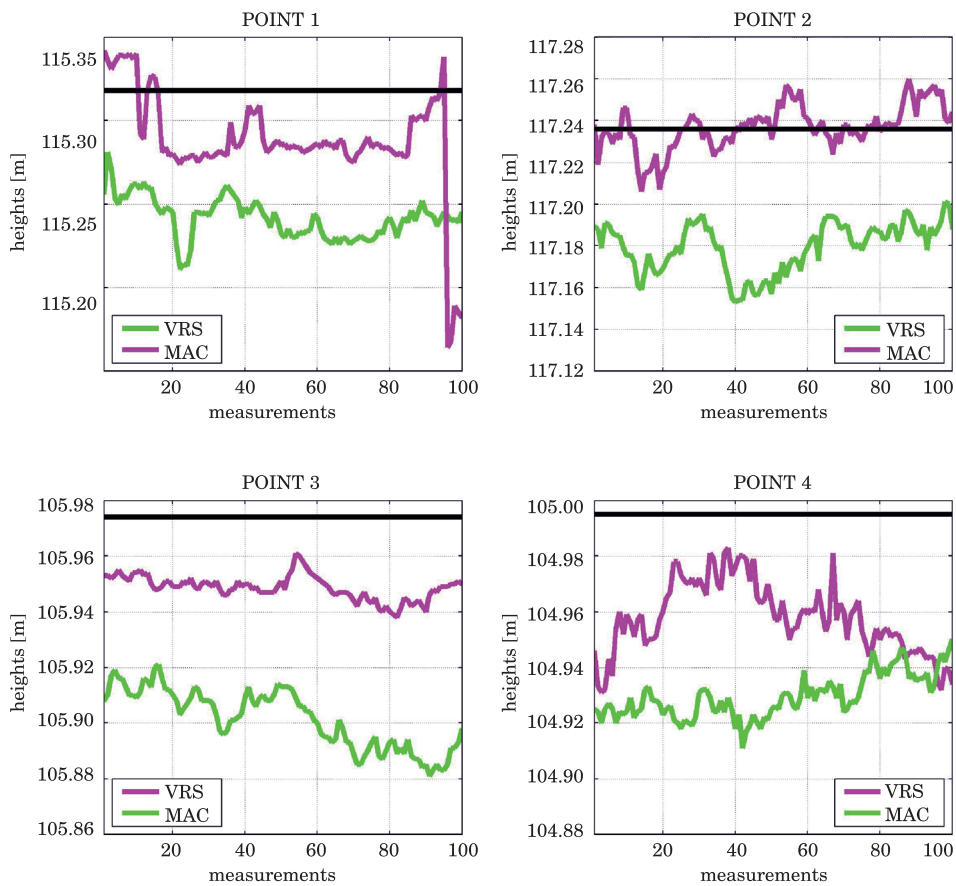
Fig. 7. Normal heights obtained from precise leveling and heights obtained from NRTK measurements in 24 May sessions
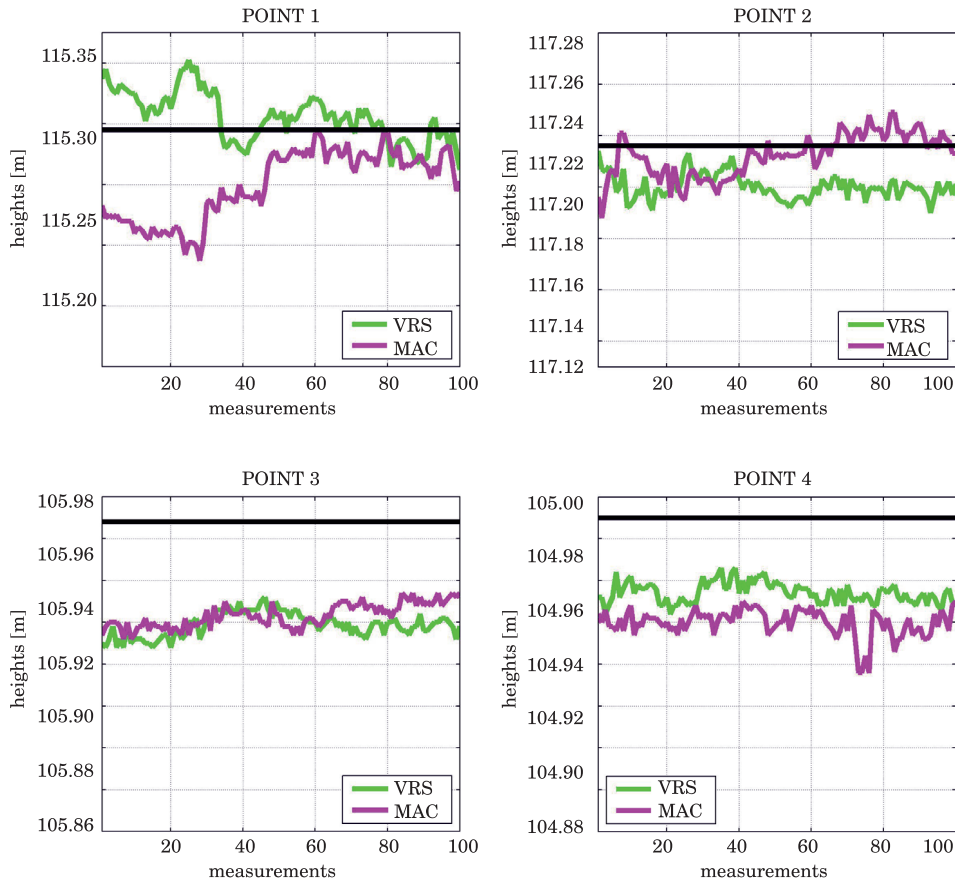
Fig. 8. Normal heights obtained from precise leveling and heights obtained from NRTK measurements in 28 May sessions

Except this case it is difficult to observe a clear effect of the level of obstacles to height determination using NAVGEO service. Results obtained for all the points have similar height variation characteristics.

It is well-known that accuracy, in our test, can be defined as how far the heights calculated during testing are from the true values for which heights from geometric leveling was adopted. Precision is a degree of repeatability that repeated measurements display, and is therefore used as a means to describe the quality of the data with respect to random errors. It was represented by the standard deviation of the solutions.

The accuracy and precision obtaining during KORTOWO test are summarised in Table 4 and Figure 9. The total accuracy of a respective point was determined as the average of the accuracy values in each session.

Sessions statistical characteristics in KORTOWO test

Specification	Session identification							
	24 March		25 March		24 May		28 May	
	VRS	SS	VRS	SS	VRS	MAC	VRS	MAC
POINT 1								
Max. height change	0.039	0.053	0.047	0.025	0.070	0.178	0.036	0.042
Standard deviation	0.010	0.011	0.010	0.005	0.012	0.032	0.008	0.011
Average height diff.	0.043	0.012	0.048	0.012	0.076	0.030	0.004	0.018
POINT 2								
Max. height change	0.046	0.049	0.051	0.022	0.048	0.054	0.041	0.024
Standard deviation	0.011	0.013	0.012	0.005	0.012	0.011	0.005	0.009
Average height diff.	0.063	0.017	0.062	0.024	0.057	0.001	0.016	0.004
POINT 3								
Max. height change	0.040	0.020	0.024	0.023	0.040	0.023	0.012	0.011
Standard deviation	0.011	0.004	0.005	0.006	0.011	0.004	0.003	0.003
Average height diff.	0.063	0.031	0.054	0.019	0.073	0.025	0.025	0.022
POINT 4								
Max. height change	0.053	0.051	0.019	0.019	0.052	0.039	0.011	0.017
Standard deviation	0.014	0.010	0.003	0.004	0.013	0.008	0.002	0.003
Average height diff.	0.056	0.024	0.052	0.017	0.037	0.066	0.018	0.025

Table 4 presents statistical analysis for the heights obtained using NRTK measurements. Analyzing results presented in Table 4 it is visible that the standard deviation, being a measure of the precision of the data, is generally in the range from 0.002 to 0.014 m (except 0001 point – MAC 24.05 session). This is due to maximum height changes from 0.011 to 0.070 m (0.178 m for 0001 point in MAC 24.05 session). Generally it can be concluded that precision of the KORTOWO test was at the centimeter level.

Average height difference, calculated as differences between geometric leveling and NRTK leveling heights, varies from 0.001 m to 0.076 m. It is noticeable that, the differences obtained in the same sessions, in most cases, are similar. This can be due to some systematic errors.

Results presented in Table 4 slightly better visualized the effect of the level of obstacles on height determination using NAVGEO service. In session VRS 25 March, MAC 24 May, VRS 28 May and MAC 28 May it visible that points marked under conditions of limited availability of satellites have worse statistical characteristics (max. height change, standard deviation) than points characterized by good measurement conditions. For the remaining four sessions results obtained for all the points have similar characteristic.

Percentage summary of difference between geometric leveling and NRTK leveling heights are presented in Figure 9.
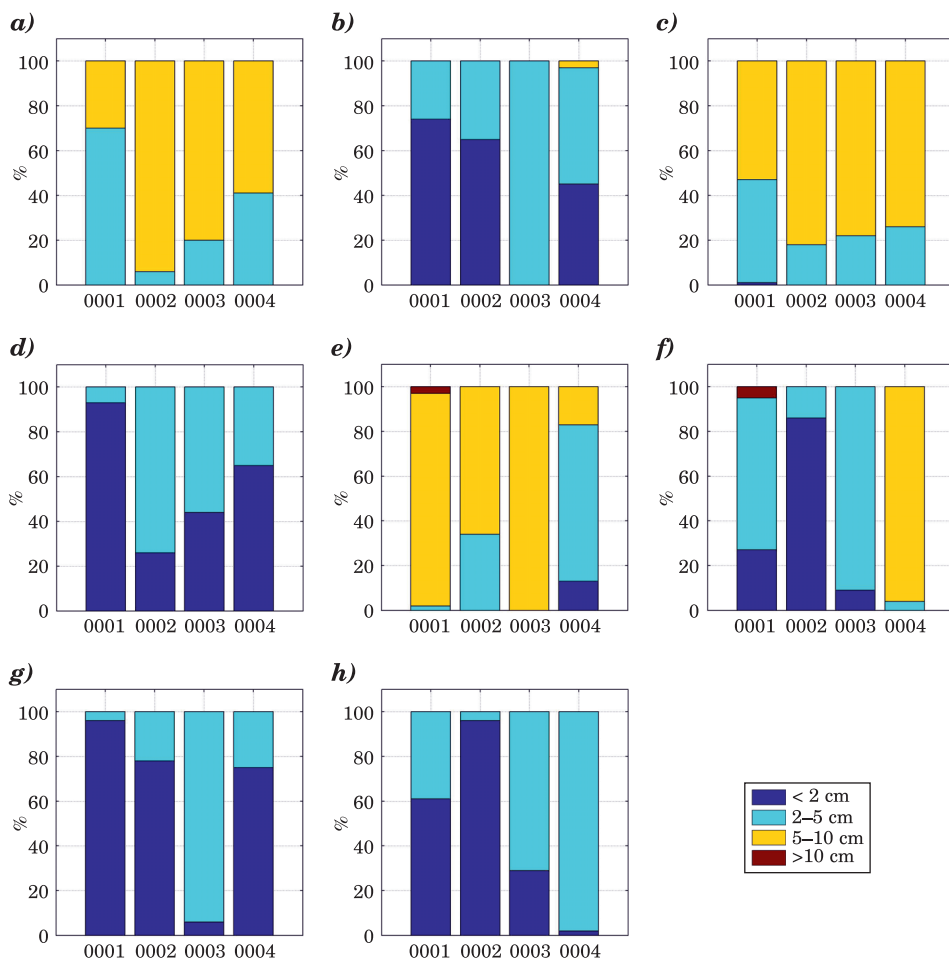
Fig. 9. Accuracy of solutions from each session for the height coordinate component: *a* – VRS 24.III, *b* – SS 24.III, *c* – VRS 25.III, *d* – SS 25.III, *e* – VRS 24.V, *f* – MAC 24.V, *g* – VRS 28.V, *h* – MAC 28.V

The accuracy obtained for the KORTOWO test varies significantly depending on the meseuring session. Generally the accuracy was better than 2 cm for an average of 31% and better than 5 cm of 71 % of the NRTK measurements.

ASG-EUPOS system uses 'QGEOID-PG̈' model (Technical Instruction G-2, 2001; Technical Guidelines G1-10, 2001, PAŻUS et al. 2002). Although this model is the result of fitting the gravimetric quasigeoid model into the satellite-levelling quasigeoid model based on points belong to e.g. the EUVN network, the EUREF-POL network or the POLREF network, almost in all sessions the systematic difference between geometric leveling and NRTK leveling heights were observed. As mentioned earlier satelite leveling can be
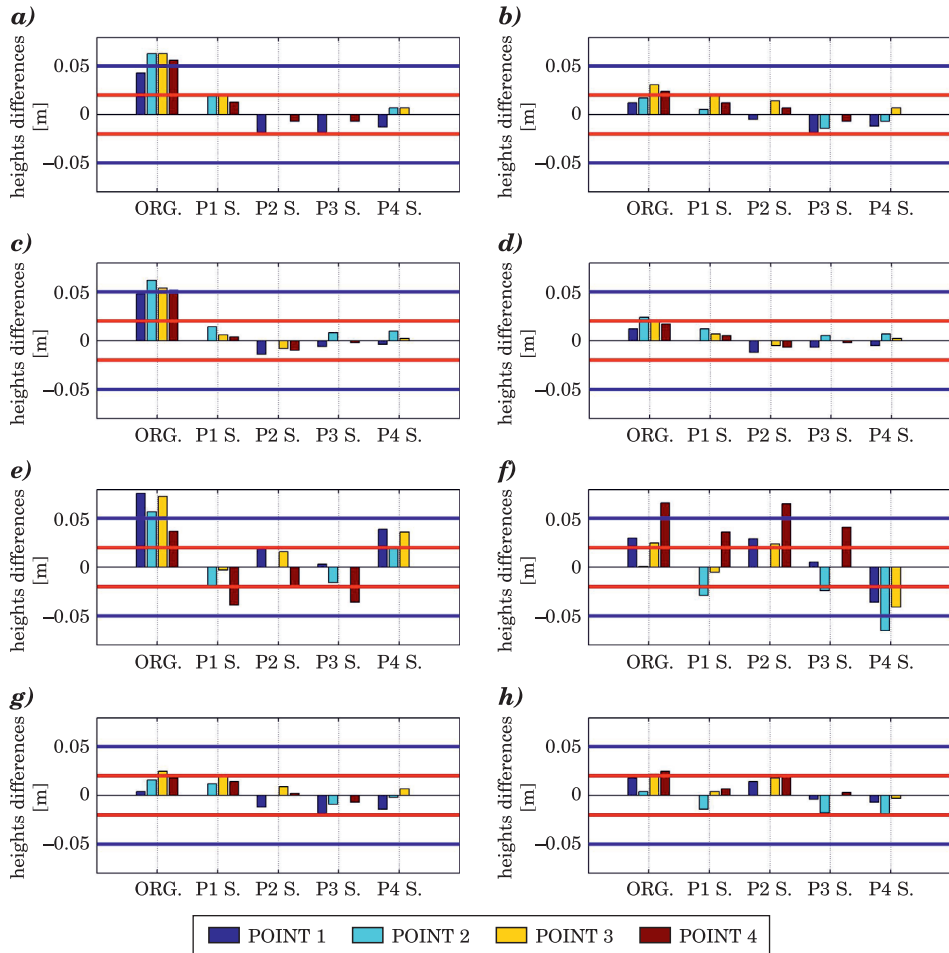
Fig. 10. Accuracy of NRTK leveling in relative approach: *a* – VRS 24.III, *b* – SS 24.III, *c* – VRS 25.III, *d* – SS 25.III, *e* – VRS 24.V, *f* – MAC 24.V, *g* – VRS 28.V, *h* MAC 28.V

done in the absolute approach, most often used in the NRTK measurements, or in relative, which due to some systematic errors that may occur in the geoid model or in GNSS measurements, is recommended by the Technical Instruction G-2. This was the reason to some additional analysis. Fitting the NRTK results to a precise leveling network was done by calculating the shift between precise leveling network surface and the NRTK height surface. The shift was calculated as the difference between the normal height from geometric leveling and height from NRTK measurements on a reference station, where each test point was successively adopted as the reference stations. Calculations were

done for all measuring epochs. The shift was then used to calculate the normal heights of the measured points – by removing it as a systematic error. Such simple fitting was done because of the small measurements area and a small number of test points. To verify the accuracy improvement the normal heights calculated in such a way were compared with the heights received from precise leveling, which were considered true. Figure 10 presents the difference between geometric leveling heights and the average NRTK fitted heights: *ORG.* – without fitting; *P1 S*, *P2 S*, *P3 S*, *P4 S* – fitted on points 0001, 0002, 0003 and 0004, respectively. Additionally, red solid lines indicate ±2 cm and blue solid lines ±5 cm differences.

From figure 10 it can be seen that fitting, as described previeously, NRTK heights to a precise leveling network, improve the heights accuracy. In the analyzed case, it is especially true for a three sessions where the worst results were obtained in *ORG.* solutions (VRS 24.III, VRS 25.III, VRS 24.V). After fitting, the height differences generally were reduced from above ±5 cm to ±2 cm. Such approach is possible only if we have bench marks in the area of our measurements. In the case where there is no possibility to connect NRTK results to leveling network a solution could be measurement using all available types of corrections. The analysis of obtained differences in the results could be helpful in identifying the best solution. In authors opinion issue of the impact of using different types of corrections in NRTK heighting is worth futher testing and analysing.

Normal heights obtained from RTK-NAWGEO leveling in TRAVERSE area are presented in figure 11. As previously, green solid lines represent heights obtained from NRTK leveling using VRS corrections, blue – using SS corrections and red – using MAC corrections. Black solid lines indicate heights obtained from precise leveling.

In analyzing the results presented in Figure 11 there are also seen some systematic differences between solutions using various types of correction. Additionally a clear trend is noticeable. Measurements done near the reference station are characterized by a higher repeatability of results than measurements made at points located more than 15 km from it. What's interesting – regardless of the type of used correction. Accuracy of NRTK heighting, which can be analyzed for the points KORT and OLST, was respectivelly ±2.6 and ±1.6 cm for VRS, ±3.0 and ±4.4 cm for SS, ±3.2 and ±4.3 cm for MAC corections.

Table 5 presents statistical analysis for the heights obtained in TRAVERSE test.
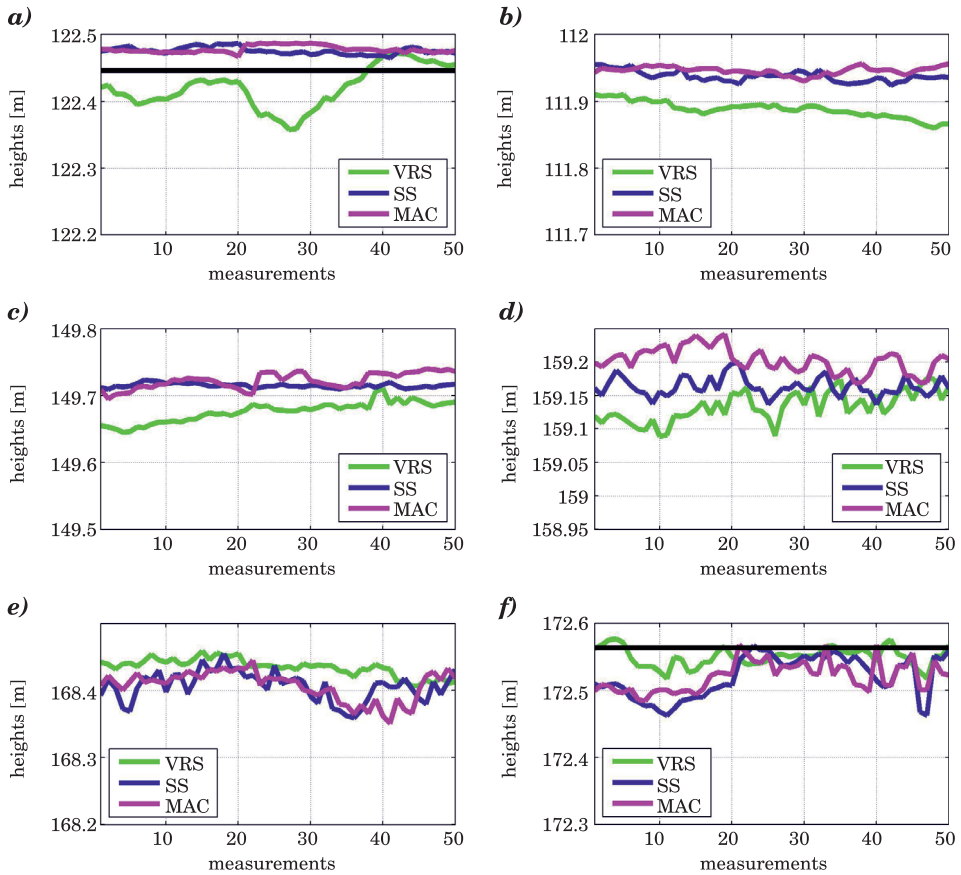
Fig. 11. Normal heights obtained from NRTK measurements in TRAVERSE area: *a* – KORT, *b* – 1001, *c* – 1002, *d* – 1003, *e* – 1004, *f* – OLST

Table 5

Statistical characteristics in TRAVERSE test

Correction typy	Point name / Characteristic type					
	KORT	1001	1002	1003	1004	OLST
Maximum height change [cm]						
VRS	11.4	5.0	6.6	8.7	4.2	5.9
SS	2.2	3.1	1.3	6.2	8.6	10.4
MAC	2.0	2.6	4.5	7.4	9.4	8.3
Standard deviation [cm]						
VRS	3.1	1.2	1.5	2.3	1.3	1.4
SS	0.5	0.8	0.3	1.4	2.2	3.2
MAC	0.5	0.6	0.9	1.9	2.2	2.2
Average normal height difference [cm]						
VRS – SS	–5.5	–5.0	–3.9	–3.5	2.8	3.0
VRS – MAC	–5.8	–5.8	–4.6	–6.9	2.7	2.9
SS – MAC	–0.3	–0.8	–0.7	–4.0	–0.1	–0.1

Results presented in Table 5 show that the distance from the nearest reference station affects the final results. It is especialy true for SS and MAC corections. The max. height changes increas from 2.2 to 10.4 cm for SS, and from 2.0 to 8.3 cm for MAC corections. For VRS corection max. height changes are at a stable, high level 7 cm on average.

In the case of standard deviation increase in value is from 0.5 to 3.2 cm for SS, and from 0.5 to 2.2 cm for MAC corections. For VRS it is generally stable and equals an average 1.8 cm.

Obtained height differences reveal also, that there are clear systematic differences between heights obtained using different types of corections. In TRAVERSE test it is especially true for VRS and other two types of corections. Heights obtained using SS and MAC corrections, unexpected because of the obvious differences in their creation, gave mostly similar results. Explanation of the reasons requires additional tests and analyzes.

Conclusions

In this paper the accuracy of the NRTK height measurements using ASG-EUPOS system was analyzed. For analysis ten points in two test areas were selected. On points some RTK measurement sessions, using three types of correction available in the NAWGEO service, were conducted. All investigations was intended to evaluate the quality of NAWGEO service from the end users' pointof view: the corrections received using the tests, accuracy analysis and additional characteristics were the same as any other subscribers would have received.

Generally, it can be conclude that RTK-NAWGEO height measurements have good precision. The standard deviations in KORTOWO test did not exceed 1.4 cm (with one exception) and the maximum height changes (with the same exception) were within 5 cm range. In one case (MAC 24.05 session), an unexpected jump in height in the 17 cm size occurred. The reason for this jump is unclear. This probably was done by undetected cycle slip or wrong ambiguity solutions. Further investigation is needed to check reasons for this type of jumps. Except this case an effect of the level of obstacles to height determination using NAVGEO service were not observed. Results obtained for all the points have similar height variation characteristics. The standard deviation in TRAVERSE test in the case of two types of corrections clearly increases with the distance to the nearest CORS station, for VRS correction it is on almost stable and equols 1.8 cm on average.

Because of the relatively low and similar value of Ionosphere Index I95 in all sessions analysis of its impact on the presented results was unjustified. The same applies to the PDOP ratio.

It was noted whereas that, there were some systematic differences between heights obtained using different types of corrections. Generally it can be assumed that, depending on the used type of correction heights can differ up to several centimeters. In authors opinion that impact of using different types of corrections in NRTK heighting requires futher testing and analysing. Performed studies are insufficient to forming the final conclusions.

In KORTOWO area there are also clear systematic differences between heights obtained using NRTK and precise leveling. This means that used type of corection can have a significant impact on obtaining heights.

The normal height accuracy, measured as a difference between NRTK and precise leveling heights, obtained for the KORTOWO test varies significantly depending on the meseuring session. The accuracy was better than 2 cm for an average of 31% and better than 5 cm of 71% of the NRTK measurements. For measurements where the largest differences occurred, fitting NRTK heights to a precise leveling network significantly improved the results. This can be done through normal height determination at least of the one point using geometric leveling. But we should remember that NRTK measurements often are fluctuating and their average also can be biased. So it would be better to used two or more points. Such approach allows for better control and adjustment of results.

If we perform measurements in the area where there are not bench marks a solution could be measurement using all available types of corrections. The analysis of obtained differences in the results could be helpful in identifying the best solution.

Acknowledgements

Translated by JOANNA JENSEN

References

APONTE J., MENG X., HILL CH., MOORE T., BURBIDGE M., DODSON A. 2009. *Quality assessment of a network-based RTK GPS service in the UK.* Journal of Aapplied Geodesy, 3 (2009): 25–34.

BOSY J., GRASZKA W., LEOŃCZYK M. 2007. *ASG-EUPOS – a Multifunctional Precise Satellite Positioning System in Poland.* International Journal on Marine Navigation and Safety of Sea Transportation, 7(4): 371–374.

BOSY J., ORUBA A., GRASZKA W., LEOŃCZYK M., RYCZYWOLSKI M. 2008. *ASG-EUPOS densification of EUREF Permanent Network on the territory of Poland.* Reports on Geodesy, 2(85): 105–112.

BROWN N., GEISLER I., TROYER L. 2006. *RTK rover performance using the Master-Auxiliary Concept, Journal of Global Positioning Systems*. 5(1–2): 135–144.

EDWARDS S.J., CLARKE P.J., PENNA N.T., GOEBELL S. 2010. *An examination of network RTK GPS services in Great Britain*. Survey Review, 42(316): 107–121.

EL-MOWAFY A. 2012. *Global Navigation Satellite Systems: Signal, Theory and Applications*. Chapter 7. Precise Real-Time Positioning Using Network RTK**,** InTech, Published.

ERHU W., HUA CH., ZHIGUO A. 2006. *VRS Virtual Observations Generation Algorithm*. Journal of Global Positioning Systems, 5(1–2): 76–81.

EULER H.J., KEENAN C.R., ZEBHAUSER B.E. WÜBBENA G., 2001, *Study of a Simplified Approach in Utilizing Information from Permanent Reference Station Arrays*. Proc. ION GPS 2001, Salt Lake City.

EULER H.J., ZEBHAUSER B., TOWNSEND B., WÜBBENA G., 2002. *Comparison of different proposals for reference station network information distribution formats*. Proceedings of ION GPS 2002, Portland, p. 2349–2358.

EULER H.J., ZELZER O., TAKAC F,, ZEBHAUSER B. 2003. *Applicability of standardized network RTK message for surveying rovers*. Proceedings of ION GPS/GNSS 2003, Portland, p. 1361–1369.

FIGURSKI M., KAMIŃSKI P., KROSZCZYŃSKI K., SZAFRANEK K. 2009. *ASG-EUPOS monitoring with referemce to EPN*. Artificial Satellites, 44(3): 85–104.

HADAŚ J., BOSY J. 2009. *Niwelacja satelitarna GNSS z wykorzystaniem serwisu NAWGEO system ASG-EUPOS*. Acta Sci. Pol., Geodesia et Descripto Terrarum, 8(2): 53–66.

HOFMANN-WELLENHOF B., LICHTENEGGER H., WASLE E. 2008. *GNSS – Global Navigation Satellite Systems*. Springer-Verlag, Wien.

Instrukcja Techniczna G-2. 2001. Szczegółowa pozioma i wysokościowa osnowa geodezyjna i przeliczanie współrzędnych między układami. Główny Urząd Geodezji i Kartografii, Warszawa.

MENG X., DODSON A., LIU C., MOORE T., HILL C. 2007. *Quality Assurance of Network RTK GNSS positioning: An End User Perspective*. Proceedings of IUGG XXIV, Perugia.

PAŻUS R., OSADA E., OLEJNIK S. 2002. *Geoida niwelacyjna 2001*. Magazyn Geoinformacyjny GEODETA, 5(84).

WANNINGER L. 1997. *Real-Time Differential GPS-Error Modeling in regional Reference Stations Networks*. Proc. IAG Symp. 118: 86–92.

WANNINGER L. 1999. *The Performance of Virtual Reference Stations in Active Geodetic GPS-networks under Solar Maximum Conditions*. Proc. ION GPS 99, Nashville, p. 1419–1427.

WANNINGER L. 2002. *Virtual Reference Stations for Centimeter-Level Kinematic Positioning*. Proc. Of ION GPS 2002, Portland, Oregon, p. 1400–1407.

WANNINGER L. 2003. *Virtual reference stations (VRS)*. GPS Solutions, 7: 143–144.

WANNINGER L. 2004. *Introduction to Network RTK*. International Association to Geodesy, Working Group 4.5.1: Network RTK, Dresden, Germany, http://www.wasoft.de/e/iagwg451/intro/introduction.html (access: 12.08.2012).

WEGENER V., WANNINGER L. 2005. *Communication Options for Network RTK*. International Association to Geodesy, Working Group 4.5.1: Network RTK, Dresden, Germany, http://www.wasoft.de/e/iagwg451/wegener/communication.html (access: 12.08.2012).

Wytyczne Techniczne G1-10: Formuły odwzorowawcze i parametry układów współrzędnych. 2001.

Wytyczne techniczne G-1.12: Pomiary satelitarne oparte na systemie precyzyjnego pozycjonowania ASG-EUPOS. 2008. http://geogis.com.pl/download/wytyczne_g_1_12_21_04_2008_1.pdf (access: 12.08.2012).

VOLLATH U., BUECHERL A., LANDAU H., PAGELS C., WAGER B. 2000. *Multi-base RTK positioning using virtual reference station*. Proceedings 13th Int. Tech Meeting Satellite Division, US ION, Salt Lake City.

Zalecenia techniczne: Pomiary satelitarne GNSS oparte na systemie stacji referencyjnych ASG-EUPOS. 2011. http://www.asgeupos.pl/webpg/graph/standards/

Zalecenia_ASG_EUPOS_20110207.pdf (access: 12.08.2012).

MODELLING BATHYMETRY CHANGES WITHIN A WATERWAY VERSUS A LABORATORY EXPERIMENT

Szymon Sawczyński[1*], *Leszek M. Kaczmarek*[2],
Jarosław Biegowski[3]

[1] Department of Mechanics and Civil Engineering Constructions
University of Warmia and Mazury in Olsztyn
[2] Department od Geotechnics
University of Technology in Koszalin
[3] Institute of Hydroengineering
Polish Academy of Sciences in Gdańsk

A b s t r a c t

A three-layer theoretical model for transport of graded sediments was used in our analysis of the silting-up of waterways tested under laboratory conditions. The experiment was conducted in a laboratory basin, in which waves and a current were generated. The current interacted with the waves propagating perpendicularly to the direction in which it was flowing. It was assumed in the calculations that the sediment was entrained from the bed and suspended due to the impact of waves on the bed, after which it was transported by the current along the cross-shore profile of the navigation channel. Thus, it was assumed that the bathymetry changes occur only as a result of changes in the suspended load transport rate. The bed topographic modifications modelling results are in good agreement to the laboratory experimental results, including the rate of silting up the waterway and the bed reconfiguration. The key factor in the calculations concerning the waterway bed reconfiguration proved to be the inclusion of the effect of sediment size sorting on predicting the rate and character of bathymetry changes.

Introduction

One of the major problems in exploitation of waterways is the maintenance of the required navigation depth. Correct prediction of bathymetry changes and the silting-up rate is of key importance. This paper is an attempt at

---
[*] Corespondence: Szamon Sawczyński, Katedra Mechaniki i Konstrukcji Budowlanych, Uniwersytet Warmińsko-Mazurski, ul. Heweliusza 4, 10-724 Olsztyn, fax 48 89 523-47-28, e-mail: sz.sawczynski@uwm.edu.pl

determination of morphological changes in a waterway bed analyzed during a laboratory experiment and compared to the results of computations. Afterwards, our results were confronted with the data reported by other researchers.

One of the conducted tests has been chosen in the analysis (T10.20.90; wave height about 0.1 m, current velocity about 0.2 m/s, wave propagation angle 90°, perpendicular to the channel – to the current flow direction). The choice was not haphazard but made in view of the fact that the results of this measurement were also analyzed in other renowned research centres (VAN RIJN 2005) under the European project SANDPIT (2002–2005) and, recently, by SANCHEZ and WU (2011). Thus, in order to be able to compare the results of our modelling test to other data, the same test was chosen.

For determination of changes in the bathymetry, a linear dependence is used that defines the relationship between a sediment transport rate and the thickness of a sediment layer composed of grains closely adhering to one another and in motion, described in greater detail by KACZMAREK et al. (2011). With this dependence, it is possible to solve an equation which describes bathymetry changes in time and space using the first-order upwind scheme. In this paper, a three-layer model of the transport of graded sediment was used for determination of the sediment transport rate and concentration of suspended sediment (KACZMAREK 1999, KACZMAREK, OSTROWSKI 2002, KACZMAREK et al. 2004).

The calculations were carried out in order to verify the model tested experimentally in a laboratory basin, where it was possible to create wave and current flow conditions with a simultaneous interaction of the current and waves propagating at an angle to the current flow direction.

Theoretical analysis, general assumptions of the model

Changes in the bed ordinate z_b after time dt can be presented as the equation:

$$z_b(x,\ t\ +\ dt) = z_b(x,\ t)\ +\ \frac{\partial z_m}{\partial t}\ dt \tag{1}$$

where

$$z_m^{+/-} = \frac{1}{(1-n_p)}\ \frac{q^{+/-}\ dt}{dx^{+/-}} \tag{2}$$

and

$$z_m = z_m^+ + z_m^- \tag{3}$$

where z_m is defined as the thickness of densely packed sediment grains which is in motion (cf. KACZMAREK at al. 2011), while q stands for the volumetric rate of

sediment transport. Besides, parameters connected with the wave crest phase are designated as $(...^+)$, whereas those associated with the wave trough phase are marked with $(...^-)$.

Dependence (2) can be converted to the form describing the sediment transport rate:

$$q^{+/-} = (1 - n_p) \, z_m^{+/-} \, \frac{dx^{+/-}}{dt} \tag{4}$$

Equation (4) under hydrodynamic equilibrium conditions (verified experimentally – KACZMAREK et al. 2011) is a linear function versus the thickness z_m but non-linear versus the ordinate z_b.

The hydrodynamic equilibrium conditions means that the flux of sediment lifted up from the bed is balanced by the flux of sediment falling down on the bottom.

Next, taking advantage of dependences (2) and (3), an equation describing bathymetry changes is obtainable, which for a two-dimensional (2-D) case can be presented as follows (SAWCZYŃSKI et al. 2011):

$$\frac{\partial z_b}{\partial t} + \frac{1}{(1 - n_p)} \left(\frac{\partial q_x^+}{\partial^+} + \frac{\partial q_x^-}{\partial^-} + \frac{\partial q_y}{\partial y} \right) = 0 \tag{5}$$

where:
z_b – bed level elevation,
n_p – porosity of bed sediment,
q_y – alongshore sediment transport rate being under hydrodynamic equilibrium conditions,
q_x^+ – mean value during the wave phase T of onshore sediment transport rate being under ąhydrodynamic equilibrium conditions,
q_x^- – mean value during the wave phase T of offshore sediment transport rate being under hydrodynamic equilibrium conditions.

In area (j,k) of the cross-shore profile, z_m layer changes within the time period Δt. Erosion or accumulation occurs due to changes in the rates of transport q_x^+ and q_x^- over the distance Δx and q_y over the distance Δy. Using the numerical upwind scheme, equation (5) can be written down with the finite difference method in a form describing the thickness of an eroded or accumulated layer for each ith fraction of the bed-forming sediment (cf. SAWCZYŃSKI et al. 2011):

$$\Delta(z_m)_{j,k}^i = \frac{\Delta t}{\Delta x} \left[(q_{bx}^+)_{j,k}^i + (q_{cx}^+)_{j,k}^i + |(q_{bx}^-)_{j,k}^i| + |(q_{cx}^-)_{j,k}^i| + |(q_{0x}^-)_{j,k}^i| - (q_{bx}^+)_{j-1,k}^i \right.$$

$$\left. (q_{cx}^+)_{j,k}^i - |(q_{bx}^-)_{j+1,k}^i| - |(q_{cx}^-)_{j+1,k}^i| - |(q_{0x}^-)_{j+1,k}^i| \right] \tag{6}$$

$$+ \frac{\Delta t}{\Delta y} \left[|(q_{0y}^-)_{j,k}^i| - |(q_{0y}^-)_{j,k-1}^i| \right]$$

where:

$$\Delta(z_m)_{j,k} = \sum_{i=1}^{N} \Delta(z_m)_{j,k}^i \tag{7}$$

The terms of the expressions marked with the indices *b, c* and *0* refer, respectively, to the bedload layer, contact load layer and outer flow region.

Within time Δt, grain-size distribution changes from $n_{j,k}^i$ to $m_{j,k}^i$ ($\Sigma m_{j,k}^i = 1$) in the control volume according to the formula (cf. KACZMAREK et al. 2004):

$$\Delta m_{j,k}^i = \frac{n_{j,k}^i (h_m)_{j,k} - \Delta(z_m)_{j,k}^i}{(h_m)_{j,k} - \Delta(z_m)_{j,k}} \tag{8}$$

In equation (8), value $(h_m)_{j,k}$ described thickness of the mixing layer, in which the grain-size distribution actually changes from $n_{j,k}^i$ to $m_{j,k}^i$ in time Δt. This change is caused by the difference in the rates of transport of particular fractions over the distances Δx and Δy.

As demonstrated by Kaczmarek et al. (2004), the mixing layer thickness can be described by the following dependence:

$$(h_m)_{j,k} = 2\frac{\Delta t}{\Delta x}[(q_{bx}^+)_{j,k} + (q_{cx}^+)_{j,k} + |(q_{bx}^-)_{j,k}| + |(q_{cx}^-)_{j,k}| + |(q_{0x}^-)_{j,k}|] + 2\frac{\Delta t}{\Delta t}|(q_{0y})_{j,k}|] \tag{9}$$

Laboratory tests have proven that the mixing layer thickness ranges from 2 cm (SISTERMANS 2001) to 5 cm (CHATELUS et al. 1998).

If we assume that the change which occurs in the analyzed control volume of the thickness $(h_m)_{j,k}$ is erosion (value of $\Delta(z_m)_{j,k}$ is positive), then, after Δt time, this erosion will form "a carpet of sediment" $a_{j,k}$ thick:

$$a_{j,k} = (h_m)_{j,k} - \Delta(z_m)_{j,k} \tag{10}$$

Thus, after Δt time, i.e. at a time moment *(t + Δt)*, a new grain-size distribution in a new mixing layer of the thickness $(h_m)_{j,k}$, will consist of the distribution $m_{j,k}^i$ found in an $a_{j,k}$ – thick carpet of sediment and the distribution $(n_s)_{j,k}^i$ characteristic of the sediment in the parent bed:

$$[n(t + \Delta t)]_{j,k}^i = \frac{a_{j,k}\, m_{j,k}^i + [(h_m)_{j,k} - a_{j,k}](n_s)_{j,k}^i}{(h_m)_{j,k}} \tag{11}$$

However, if we assume that within the analyzed area sediment accumulation rather than erosion takes place (value $\Delta(z_m)_{j,k}$ is negative), the new grain-

size distribution after Δt time at a time moment $(t + \Delta t)$ in a new mixing layer of the thickness $(h_m)_{j,k}$ will consist exclusively of the distribution $m_{j,k}^i$ found in a carpet of sediments of the thickness $a_{j,k}$.

In a situation where, for example, a wave propagates along the waterway (parallel to its longest axis) without causing any changes in the bathymetry in that direction (when waves are formed over a shallow bottom, no bathymetry changes take place), and the direction of the current flow is perpendicular to the direction of waves, then the problem is reduced to a two-dimensional one. The question formulated as above means that the evolving considerations will concern exclusively the effects produced by the alongshore current, which means that we will have to leave out the terms connected with wave formation and the offshore current from equations (5), (6), and (9).

The rate of the alongshore sediment transport which takes place in the outer flow region can be presented as (SAWCZYŃSKI et al. 2011):

$$q_{0y} = \int_{\delta_{cr}}^{h} U_{0y}(z) \langle C_0(z) \rangle \, dz \tag{12}$$

where:
h is the depth of water, δ_{cr} is the upper boundary of contact load layer – shared by all fractions (KACZMAREK 1999) and velocity $U_{0y}(z)$ is the velocity of the alongshore current.

In order to achieve the averaged over time T value of the concentration $\langle C_0(z) \rangle$ of suspended sediment mixture, the following dependence is used (cf. e.g. RIBBERINK, AL-SALEM 1994):

$$\langle C_0(z) \rangle = \langle C_0(z = \delta_{cr}) \rangle \left(\frac{\delta_{cr}}{z}\right)^{\alpha_1} \tag{13}$$

where concentration on the reference level (δ_{cr}) is determined by averaging over the wave phase the results obtained for the contact load layer (c_c):

$$\langle C_0(z = \delta_{cr}) \rangle = \sum_{i=1}^{N} \langle c_{ci}(z = \delta_{cr}, t) \rangle n_i \tag{14}$$

BIEGOWSKI (2006) established the value of the exponent at $\alpha_1 = 0.6$.

The values of concentration c_{ci} in the contact load layer for all fractions of the sediment, averaged over the wave phase, are established according to the three-layer model of graded sediment (KACZMAREK 1999, KACZMAREK, OS-TROWSKI 2002, KACZMAREK et al. 2004).

Description and conditions of the laboratory experiment Test 1

The laboratory measurements (HAVINGA 1992, WALSTRA et al. 1999) were completed at WL | Delft Hydraulics (current name Deltares) located in the north of the Netherlands.

Directional waves, in the form of the JONSWAP spectrum of the frequency peak 0.4 Hz, were generated. A system of pumps was used to create a current in the basin. The water depth was about 0.4 m. The canal was filed with sediment in its terminal part, and the bed consisted of fine sand (d_{50} = 100 µm; d_{90} = 130 µm), lying on the same level as the concrete floor of the basin around the channel. A detailed description of the Test 1 experiment was given by HAVINGA (1992).

The bed was shaped in the sand layer so as to resemble a navigation channel. Changes in the ordinates of the bed were monitored by regular soundings of the bed for over 25 hours in three measurement sections (Fig. 1). The measurements of the initial profile were as follows: depth about 0.2 m, bed width about 0.5 m and side slopes about 1 : 8. The trench (the longest axis) was situated normal to the current and parallel to the direction of wave propagation, cf. Figure 1.
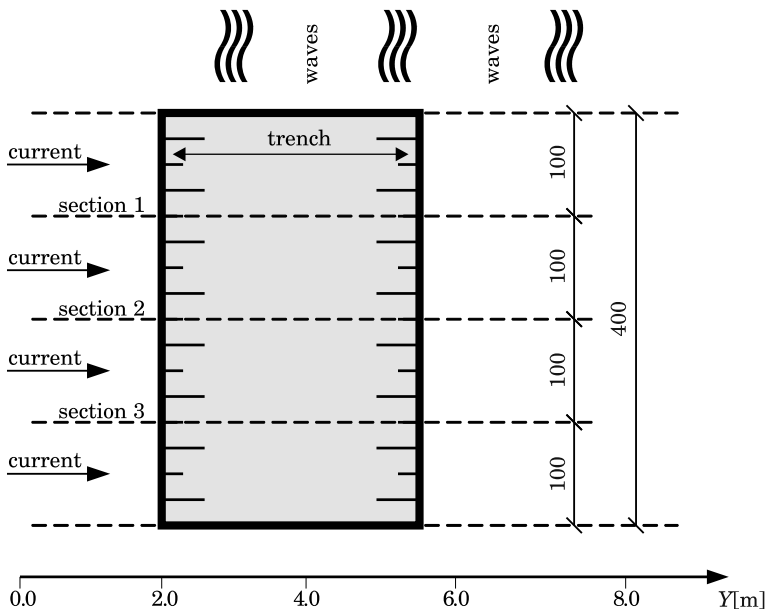

Fig. 1. Design of the Test 1 experiment

Source: HAVINGA (1992)

The basic parameters measured on the inflow side during the experiment are presented in Table 1.

Table 1

Basic parameters of the Test 1 experiment

Parameter	Symbol	Value	Unit
Water depth	h_0	0.42	[m]
Significant wave height	H_s	0.105	[m]
Peak wave period	T_p	2.2	[s]
Depth – mean current velocity	u_0	0.245	[m/s]
Angle between current and waves	α	90	[°]
Representative particle size of bed	d_{50}; d_{90}	0.10; 0.13	[mm]
Fall velocity of suspended sediment	w_s	0.006	[m/s]
Suspended sand transport	$q_{s,o}$	0.018 – 0.024	[kg/s/m]
Ripple height	–	0.007	[m]
Ripple length	–	0.084	[m]
Sediment density	ρ_s	2650	[kg/m³]
Fluid density	ρ_w	1000	[kg/m³]
Porosity of bed material	n_p	0.4	[–]

Source: HAVINGA (1992)

Modelling distributions of the vertical concentration of suspended sediments

A three-layer model of the graded sediment transport (KACZMAREK 1999, KACZMAREK, OSTROWSKI 2002, KACZMAREK et al. 2004) is used for mathematical modelling of the vertical concentration of suspended sediment, which needs to be known in order to determine the sediment transport rate in the outflow region described by equation (12).

Two available parameters, i.e. representative diameters d_{50} and d_{90}, were taken as input data for sediment. By knowing these data, we were able to plot the input grain-size distribution curve, shown in Figure 2. The grain-size distribution shown in this paper was used in calculations for Test 1 experiment (HAVINGA 1992) and Test 2 experiment (VAN RIJN 1985), which were analyzed in a paper by SAWCZYŃSKI et al. (2011). Both experiments were also thoroughly discussed under the international project SANDPIT (VAN RIJN 2005).

Due to the narrow range of diameters of the fine sediment used in the experiment, three representative diameters, reflecting the lower values of the diameter interval ranges shown as a histogram in Figure 2, were taken for the calculations. The lower threshold values of these intervals correspond to the control sieve mesh sizes.
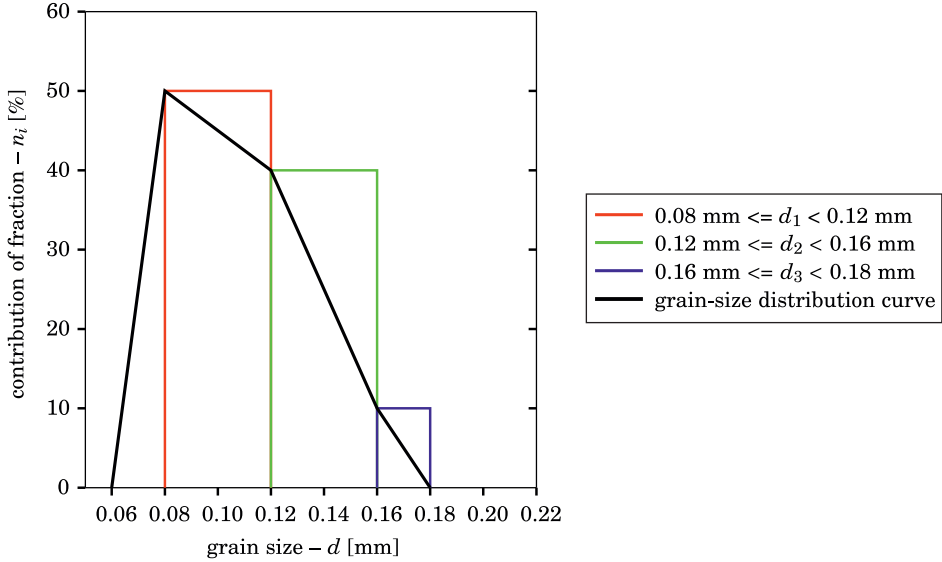
Fig. 2. Histogram of grain-size distribution according to d_{50} and d_{90}, used in the calculations

The mathematical modelling of the vertical concentration of suspended sediments was accomplished for a regular, symmetric (sinusoid) wave described by two parameters: root mean square wave height (H_{rms}) and zero-crossing wave period (T_z). The computed vertical concentration distributions were then compared with the results obtained during the experiment at a cross-section located at the beginning of the canal ($y=0$) before the model.

The measurement data from the experiment enabled us to analyze vertical distributions of the suspended sediment concentrations under weak hydrodynamic conditions. The dimensionless friction calculated only for the wave formation conditions (excluding the effect of a current), most often described by Shields' parameter $\Theta_{2.5}$ (calculated for $d_{50} = 0.10$ mm), assumed the values within $0.08 < \Theta_{2.5} < 0.12$. These values of Shields' parameter then indicate that the bed was rippled throughout the experiment (cf. Table 1).

Figure 3 shows a graphic comparison of the calculated vertical suspended sediment concentration profile versus the profile measured during the Test 1 experiment (HAVINGA 1992, WALSTRA et al. 1999). Calculations of the concentrations were completed based on the initial data contained in Table 2 and the bed grain-size distribution curve, as shown in Figure 2.

Basic entry data used for modelling vertical concentration of suspended sediment and bathymetry changes

Parameter	Symbol	Value	Unit
Water depth	h_0	0.42	[m]
Root mean square wave height	H_{rms}	0.074	[m]
Zero – crossing wave period	T_z	1.86	[s]
Representative particle size of bed	d_{50}; d_{90}	0.10; 0.13	[mm]
Sediment density	ρ_s	2650	[kg/m^3]
Fluid density	ρ_w	1000	[kg/m^3]
Porosity of bed material	n_p	0.4	[–]

Figure 3 shows that the concentration of suspended sediments was not measured at a distance very close to the bed. The authors could not measure concentrations near the bed due to the varied and above all considerable height of ripples observed during the tests.
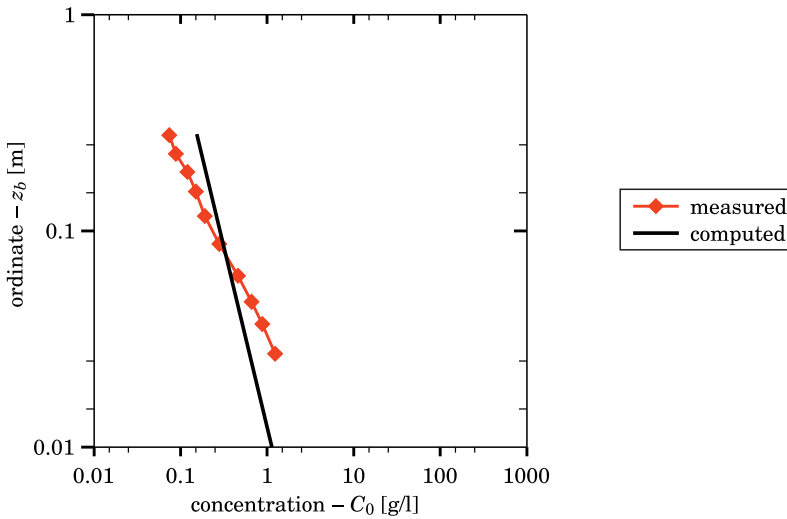

Fig. 3. Comparison of the computed (present model) and measured vertical profile of suspended sediment concentrations

Source: HAVINGA (1992)

In Figure 3, a slight difference is visible between the inclination angles of the graph drawn along the measurement points and the one obtained from the calculated sediment concentrations. At a height of about 7.5 cm (from the bed), the graphs intersect with each other, which obviously means that the cal-

culated and measured values are identical. At a distance closer to the bed, the measured concentration values are slightly higher than the ones calculated from the theoretical model, whereas at a larger distance, they are slightly smaller. This slight discrepancy of the results may be due to the fact that the analyzed hydrodynamic conditions were very weak and the bed was rippled.

Besides, as has been demonstrated by BOSMAN (1982, 1985), local and instantaneous measurements of concentration are typically burdened with high and random variability of results, ranging from 50 up to 100%. The main reason for such high variability of measurements is the strong influence of local conditions, especially near the bottom. In order to minimize such differences in measured concentrations of sediments, time- and space-averaged results are considered. Although the results are averaged, the differences may remain significant when the bed is rippled.

Considering the above, as well as any error possibly hidden in the measuring method used in the experiment, it is possible to claim quite confidentially that the coincidence between the measurements and the results calculated from the proposed theoretical model is satisfactory.

Modelling bathymetry changes and sediment grain size distributions

The process of modelling of bathymetry changes consisted of two major stages:
– excluding the effect of changes in the sediment grain-size distribution during the bed reconfiguration process,
– including the effect of size sorting on the bed reconfiguration.

A three-layer model of graded sediments transport (KACZMAREK 1999, KACZMAREK, OSTROWSKI 2002, KACZMAREK et al. 2004) was used for determination of the sediment transport rates. Two available parameters, i.e. representative diameters d_{50} and d_{90}, were taken as entry data in the mathematical modelling of bathymetry changes and the sediment grain-size distribution. The grain-size distribution curve can be seen in Figure 2. The basic entry parameters used for calculations are presented in Table 2. Other data included in the calculations are the angle between the current flow direction and the wave propagation direction, $\alpha = 90°$ (normal to the waves) and depth-averaged velocity of the current $u_0 = 0.245$ m/s, related to the water depth $h_0 = 0.42$ m (cf. Figure 5). This current is identifiable with an alongshore current, characteristic for coastal zones. The graph showing changes in the calculated mean velocity of the alongshore current along the initial profile of the bed (for time simulation $t = 0$), depending on the water depth, is given in Figure 4.
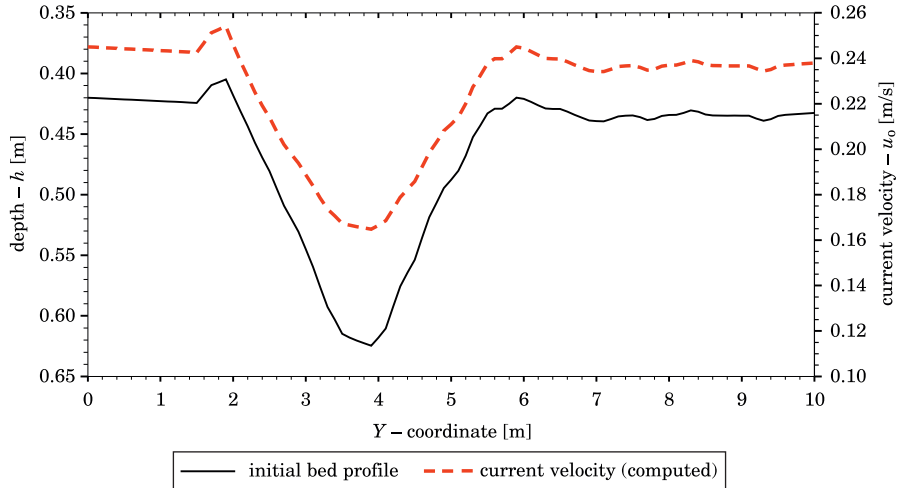
Fig. 4. Variability of the calculated alongshore current velocity in the initial bed profile depending on the water depth – experiment Test 1

Moreover, in our calculations of changes in the bed morphology and changes in the sediment grain-size distribution, we assumed that sediment is entrained from the bed into the suspension state only by the impact of waves onto the bed. Next (considering a two-dimensional case), the load lifted from the bed is transported by the current along the cross-shore profile of the navigation channel. Thus, it was assumed that modifications of the bed occur as a result of changes in the rate of suspended sediment transport.

Calculation procedure

It was decided that the spatial simulation would begin at the coordinate $y = 0.0$ m, and finish at $y = 10.0$ m, cf. Figure 5. The computational step in space was taken as 0.1 m, as a result of which 101 measuring points were achieved, including two extreme ones on the boundaries of the modelling area. In order to determine the sediment transport rate, the vertical interval was set up from the depth of $h = 0.35$ m to $h = 0.65$ m. This interval was divided into minute layers, each of the thickness equal the computational step in space, i.e. $\Delta h = 0.001$ m, and then, for each of the layers, the sediment transport rate was established.

The determination of the computational step in time Δt was accomplished based on the calculations derived from the assumption that the mixing layer thickness described with equation (9), determined in locations where the water depth was the smallest (i.e. the sites where the hydrodynamic impact on the

bed was the strongest) was approximately 2.0 cm (including the porosity of the
sediment, approximately 3.3 cm). From the transformation of equation (9), the
computational step in time was calculated to equal Δt = 90 s.
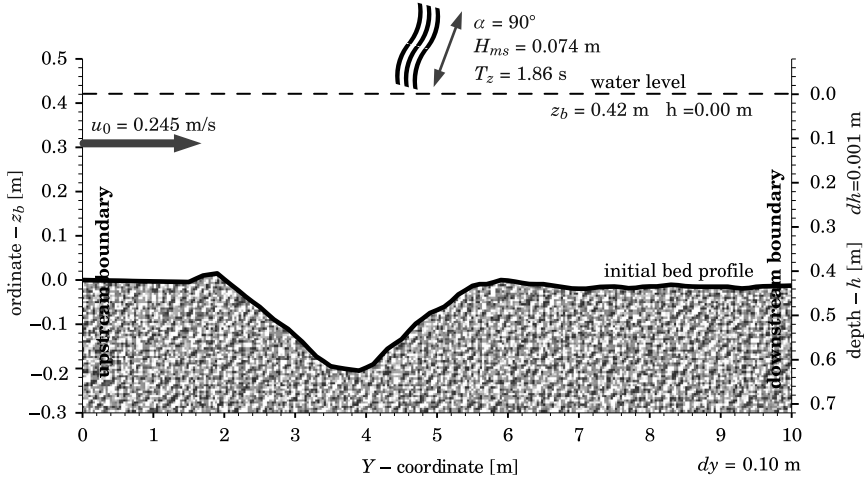

Fig. 5. Entry data for calculations of bathymetry and grain-size distribution changes

On the left-hand side margin of the solution area y = 0.0 m, for the
sediment transport in the direction of the current flow, when $q_y > 0$, a marginal
condition $z_b(y = 0, t) = z_{b(0)}$(t) = 0.000 m was set (corresponding to the water
depth of h_0 = 0.420 m), for time $t \geq 0$.

As the navigation channel is silted up exclusively due to the impact of the
current (a two-dimensional problem), equation (5) is simplified by zeroing out
the wave-derived terms q_x^+ and q_x^-, which consequently leads to a one-stage
solution of equation (5) describing bathymetry at each time level Δt.

Thus, at each time level, equation (5) is solved, simultaneously setting the
initial condition: $z_b(y,t) = z_b^{(t=0)}$, with the function $z_b^{(t=0)}$ describing the initial
bathymetric profile of the flume imitating a navigation channel, and the
marginal condition on the left-hand side boundary: $z_b(y = 0, t) = z_{b(0)}$(t) = 0.000 m.
Moreover, it has to be noticed that no condition is set for the right-hand side
boundary.

For determination of a new grain-size distribution after Δt time, at a time
moment $(t + \Delta t)$ in a new mixture layer of the thickness $(h_m)_{j,k}$, calculations are
made based on some of the equations from (6) to (11) chosen depending on
which process – accumulation or erosion – occurs at a given point. It should be
underlined that the scope and course of the experiment (cf. Fig. 1 and Fig. 5.)

make us adopt a simplification in differential equations (6) and (9) consisting in the omission of the terms connected with waves and the offshore current.

Next, calculations are carried out at the subsequent time step $(t + \Delta t)$ and the whole process is terminated once the final simulation time T is reached.

Comparison of the results of modelling bathymetry changes for uniform sediment with the experimental data

In the first stage of modelling the bathymetry evolution, calculations were carried out without taking into account changes in the bed grain-size distribution, which take place in response to changes in the sediment transport rate.

It was assumed that the bed was composed of uniform sediment, i.e. of grains of an identical diameter. The duration of the simulation event was 25.5 hours. Calculations were carried out for four situations, i.e. the bed was composed of grains of the diameter (i) $d = 0.08$ mm, (ii) $d = 0.10$ mm, (iii) $d = 0.13$ mm, (iv) $d = 0.16$ mm. Fig. 6 shows the results of the modelling of the sediment transport rate for the beds initial profile, i.e. for time $t = 0$ and for uniform sediment and four grain diameters.
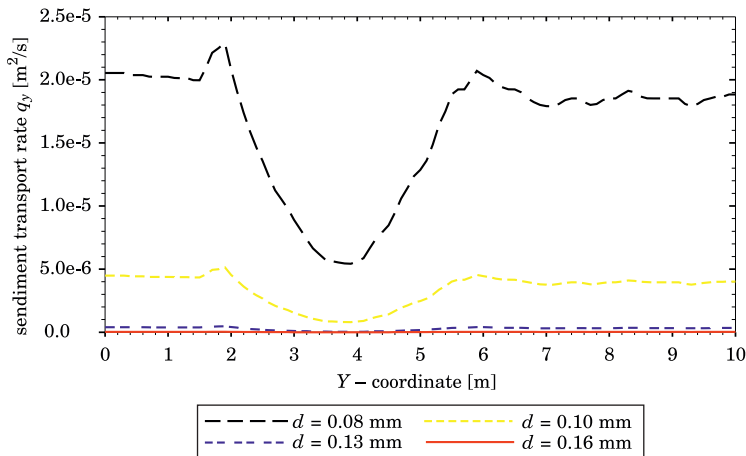

Fig. 6. Results of modelling of the sediment transport rate for the bed's initial profile, and for uniform sediment

The results of the modelling of changes in the bed's morphology for uniform sediment are presented in Figure 7. Because fine sediment fractions are transported much more intensively than coarser ones, the modelling of changes in the bed's morphology for the finest sediment ($d = 0.08$ mm) leads to the navigation channel being completely silted up. For the coarsest fraction ($d = 0.16$ mm), which remains immobile, that is does not participate in the

sediment transport under the effect of hydrodynamic forces at deeper water depths (cf. Fig. 6), no bathymetry change is practically observable. For grains of the diameter $d = 0.13$ mm, the sediment transport rate is slightly higher than calculated for grains measuring 0.16 mm in diameter, which also caused small changes in the reconfiguration of the waterway bed.
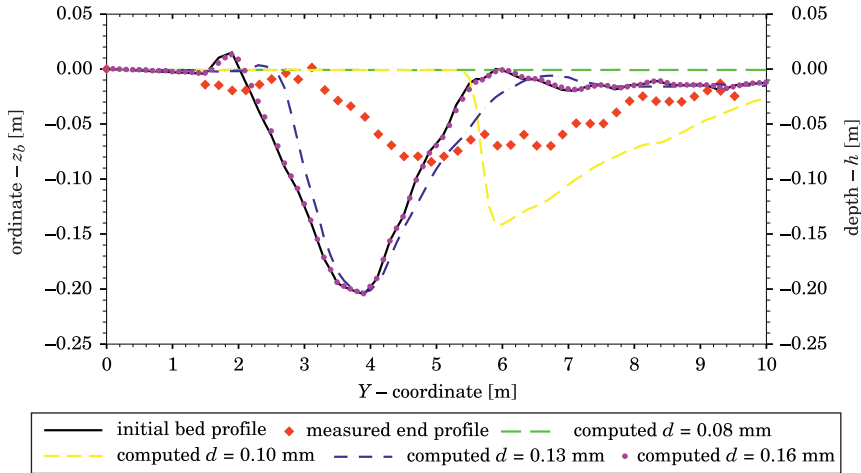

Fig. 7. Changes in the bed profile after $T = 25.5$ hours. Comparison with the results of the modelling for uniform sediment

Considering the above information and the data presented in Figure 7 corresponding to the changes in the bed profile after time T = 25.5 hrs for uniform sediment, it can be concluded that none of the results of calculations of the changes in the bed's morphology, at any of the tested situations, is a reflection of the results achieved during the measurements. Even if we take into consideration the representative diameter of sand grains, such as $d_{50} = 0.10$ mm, the results of modelling changes in the level of the bed of the navigation channel are far different from the results obtained during the laboratory experiment.

Effect of the sediment sorting on the bathymetry changes

During the second stage of modelling bathymetry changes, the calculations included the effect of sediment sorting on the reconfiguration of the bed. An additional analysis was performed for a case where sediment consisted of a mixture of three fractions (cf. Fig. 2) but changes in its grain-size distributions were not included into the calculations. Thus, it was assumed that at all points of calculations, located along the length of the cross-shore profile and during the

whole time of the simulation experiment, the bed was composed of the load whose grain-size distribution was constant and identifiable with the original sediment.

Figure 8 shows a comparison of the modelling results with the measurements of the final bathymetry (after time $T = 25.5$ hrs) of the navigation channel. The results of calculations for sorting and non-sorting sediments were distinguished. Figure 9 illustrates the final changes in grain-size distributions, where – additionally – the initial grain-size distribution (for time $t = 0$) was shown (thin, dotted, horizontal lines).
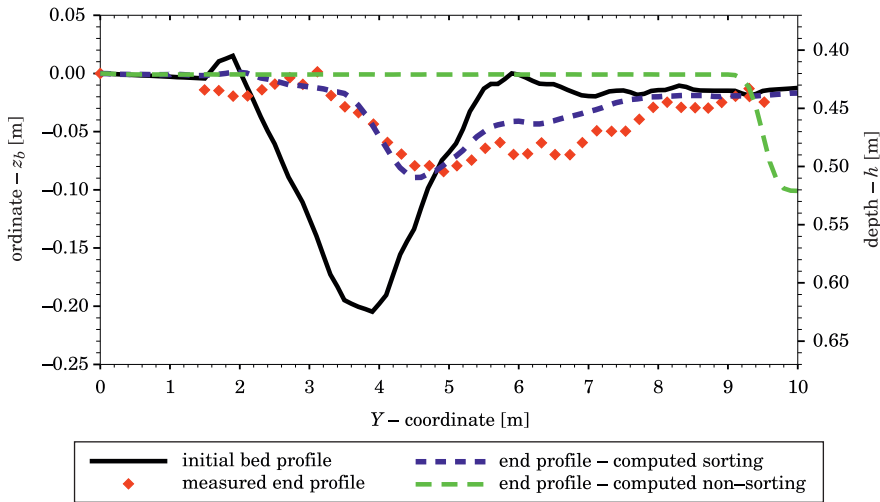
Fig. 8. Comparison of the results of modelling changes in the bed level with measurements after time $T = 25:30$ h
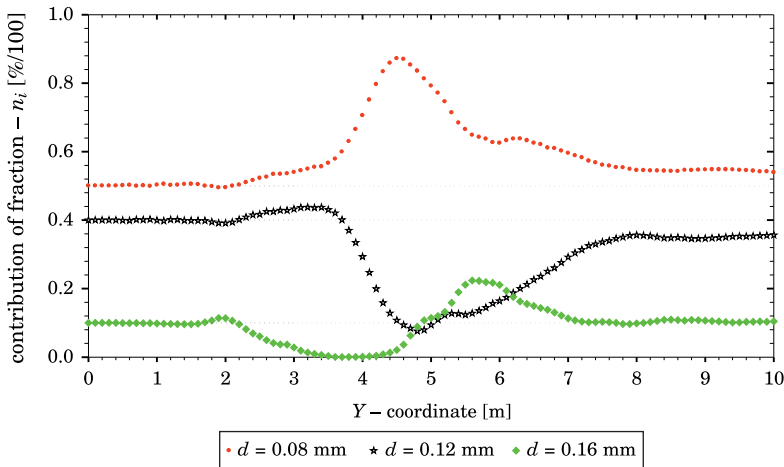
Fig. 9. Results of modelling changes in the grain-size distribution after time $T = 25:30$ h

The bed morphology modifications modelling results demonstrates that the navigation channel migrates towards the direction of the current. With the current flow conditions throughout the experiment, the resultant sediment transport (understood as a difference in the transports of all the sediment fractions at points *j* and *j-1*) assumes positive values on the downstream slope (cf. Fig. 6), thus increasing the depth, that is causing erosion of the bed. A reverse situation can be observed on the upstream slope. The resultant sediment transport achieves negative values and therefore the depth decreases, which means deposition of sediment.

The results of our modelling of the changes in the morphology of the bed over time show that when the process of sediment grading is not included in calculations then changes in the bed shape occur much faster than the measured results. Also, the character of bed reconfiguration is different. Noteworthy is an exceptionally large angle of the inclination of the upstream slope as well as a high rate of migration, which is so fast that eventually the navigation channel is far outside the scope of measurements.

Recapitulating, when the calculations do not account for changes in the grain-size distribution of the sediment, then the rate of migration of the canal is too fast and – at the same time – the rate of the accumulation process, which slows down the migration of the canal and causes the silting-up of the waterway, is too slow.

As Figure 6 demonstrates, at the biggest depths tested during the experiment, only the finest fractions were transported while the coarse ones did not participate in motion. In areas of the highest deposition, where practically only the finest fraction ($d = 0.08$ mm) is transported (Fig. 6), a considerable increase in its percentage in the total grain-size distribution is observed, until reaching the maximum value for the whole profile, and a simultaneous decrease in the share of fractions $d = 0.12$ mm and $d = 0.16$ mm occurs. In the areas subjected to maximum erosion, the material is becoming coarser, a development confirmed by a decreasing tendency in the contribution of the finest fraction $d = 0.08$ mm, a decrease in the percentage of fraction $d = 0.12$ mm and a large increase in the share of the coarsest fraction $d = 0.16$ mm, up to the highest value for the whole profile.

Bathymetry changes – comparison with the modelling results

Tests on calibration and improvement of own mathematical models has been undertaken by acclaimed research centres participating in the international project SANDPIT (VAN RIJN et al. 2005, WALSTRA et al. 2005). The models were scaled on two planes, i.e. 'A' and 'B', in order to 'adjust' the

results of modelling to the results achieved during a laboratory experiment (VAN RIJN et al. 2005, WALSTRA et al. 2005). The 'A' problem concerned the adjustment of results of calculated changes in the bed's bathymetry according to the measured values of the sediment transport rate; the other approach ('B') dealt with observations of changes in the bed's morphology over time. Comparison of the results of calculations of bathymetry changes based on the authors' own mathematical model, versus some previous results achieved once the mathematical models suggested and tested by the SANDPIT project participants had been scaled, is illustrated in Figure 10 (approach 'A') and Figure 11 (approach 'B'). More details on the process of scaling the mathematical models can be found in the articles by WALSTRA et al. (2005) and VAN RIJN et al. (2005).
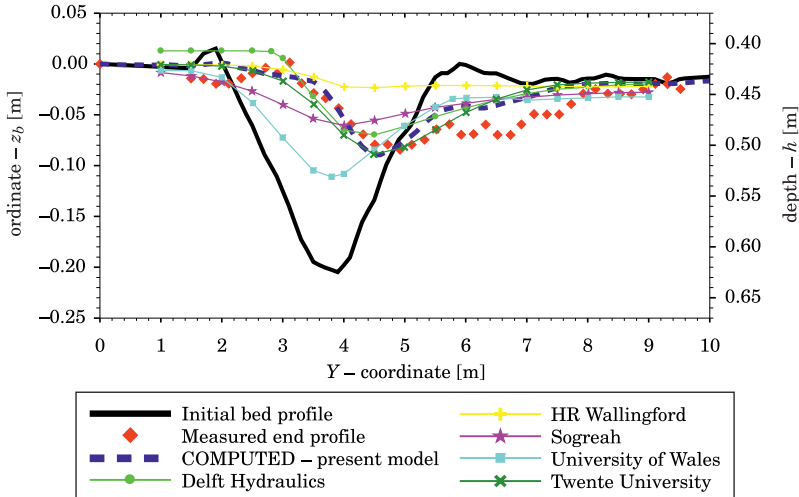

Fig. 10. Comparison of the results of modelling bathymetry changes after time T = 25:30 hours. Approach 'A' – calibration of models performed by the SANDPIT project participants based on measured sediment transport rates

Figure 10 and Figure 11 show that none of the models tested under the SANDPIT project was able to correctly predict erosion and flattening on the downstream slope or estimate the rate of migration and nature of changes of the downstream slope of the navigation channel. It was also interesting to notice that calibrations of the models carried out according to the observations of changes in the bed's morphology in time and space did not result in attaining a better agreement between the results of calculations and measurements of the end morphology.
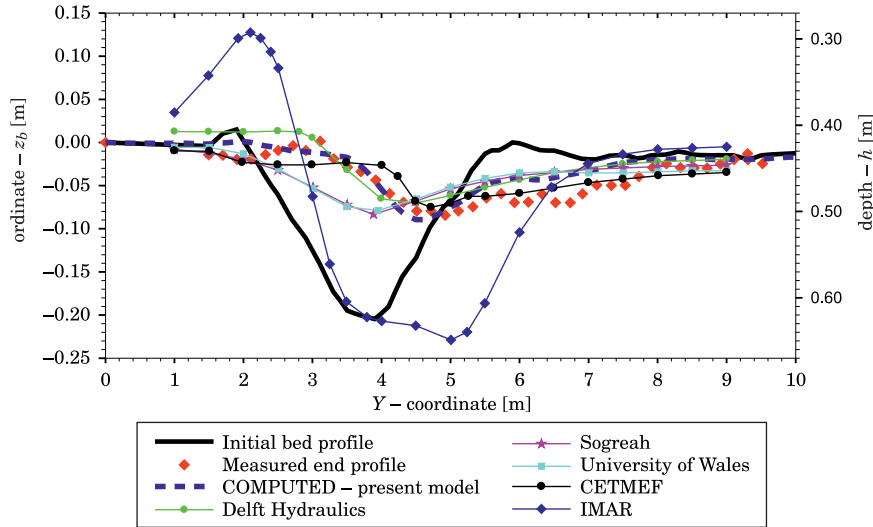
Fig. 11. Comparison of the results of modelling bathymetry changes after time T = 25:30 hours. Approach 'B' – calibration of models performed by the SANDPIT project participants based on observations of changes in the bed's morphology

Recently, SANCHEZ and WU (2011) showed some interest in the experiment called Test 1. Analogously to researchers participating the SANDPIT project, they decided to verify their own model with reference to the results obtained from the laboratory measurements. Some important conclusions can be found in their article (SANCHEZ and WU 2011). Comparison of the results of modelling bathymetry changes over time T = 25:30 hours and the results obtained by SANCHEZ and WU (2011) versus the results derived from the laboratory measurements are shown in Figure 12.

This comparison is impressive but we should bear in mind that the solution reported by SANCHEZ and WU (2011), analogously to the other models cited in this paper, does not provide us with any information regarding changes in bed grain-size distributions within the navigation channel or its environs.

Such information, however, is given by the mathematical model presented in this paper. Thus, it is worth noticing once more a much better agreement between the bathymetry changes computed when a higher number of fractions in the bed grain-size distribution is included versus the measured data than achieved with the model used in Test 1 experiment and presented by SAW-CZYŃSKI et al. (2011) or the model in Test 2. Figure 13 shows two slightly different variants of bed grain-size distribution consisting of far more fraction intervals (seven instead of three in Fig. 2), but also preserving the indices characteristic for d_{50} and d_{90}, i.e. d_{50} = 100 μm as well as d_{90} = 130 μm.

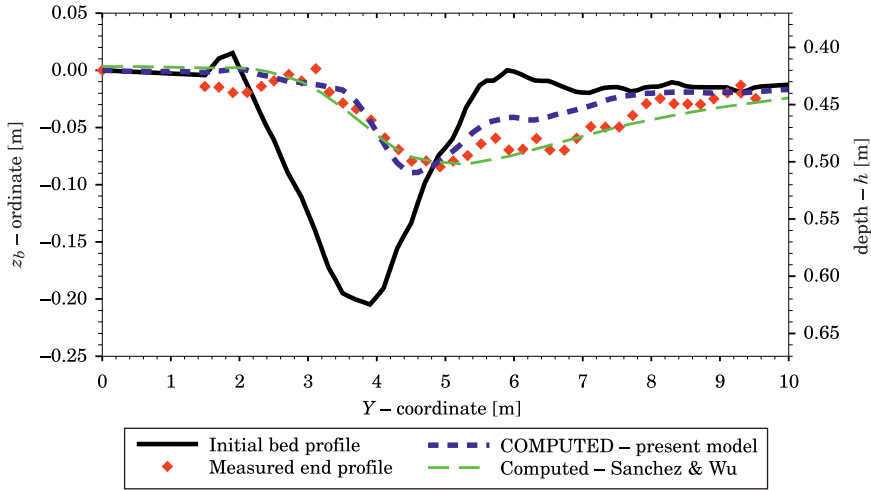Fig. 12. Comparison of the results of modelling bathymetry changes after time T = 25:30 hours with the measurements and the results obtained by SANCHEZ and WU (2011)
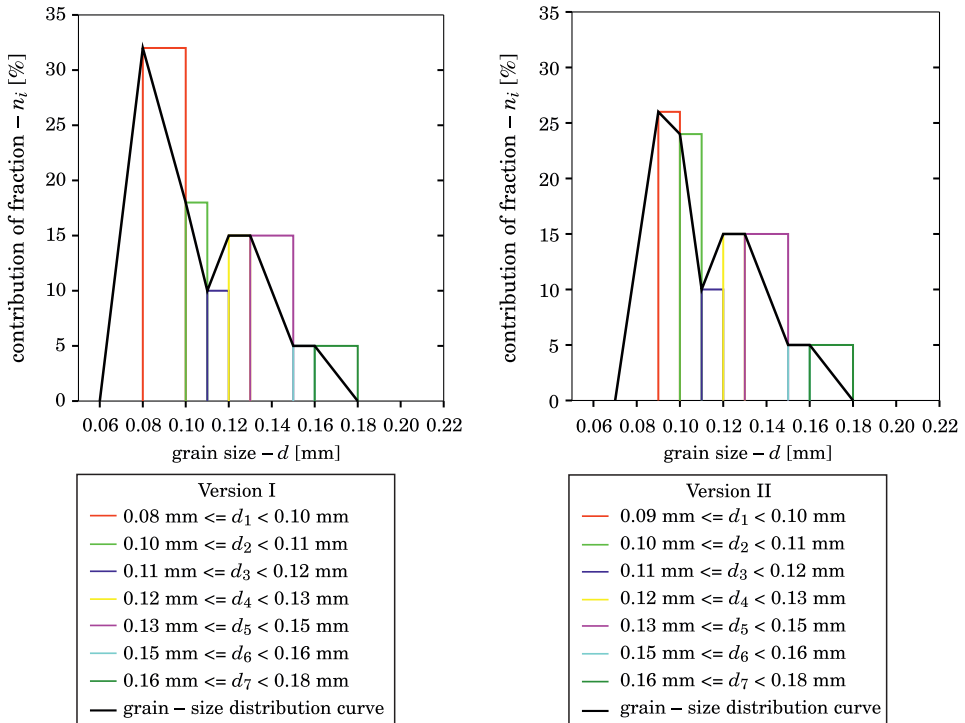

Fig. 13. Histograms of two variants of bed grain-size distribution according to indices d_{50} and d_{90}, included in calculations in order to attain the most precise reflection of the results of bathymetry changes obtained by taking measurements

Figure 14 illustrates results of modelling changes in the bed's morphology using these grain-size distribution patterns.
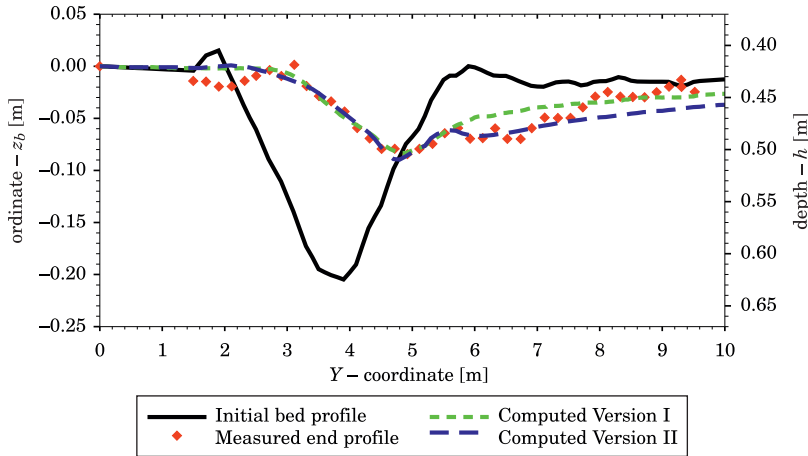

Fig. 14. Comparison of results of modelling bathymetry changes after time $T = 25:30$ hours with results of measurements. An attempt at the possibly most precise reflection of results of bathymetry changes obtained during measurements

By introducing into calculations a higher number of grain fractions, it was possible to improve considerably the results of modelling changes in the bed configuration on the downstream side, i.e. to increase its erosion. At the same time, it was observed that the results for the upstream side slightly improved. The results of calculations carried out for two variants of bed grain-size distribution are a kind of an envelope within which the experimental results are successfully fitted. It is therefore concluded that the precision of computed bathymetry changes improves as the number of sediment grain fractions included in a modelling effort is higher. The effect of sediment grain-size distribution on the rate and character of the bed profile reconfiguration remains very important.

Summary

When comparing results of computations of bathymetry changes of a waterway, excluding or including the effect of changes in the sediment grain-size distribution modifications on the bed reconfiguration, it can be noticed and should be emphasized that the latter are in a better agreement with the results obtained from laboratory measurements. The agreement was

further improved when the number of sediment grain fractions was higher. Thus, it is advisable to underline the significant effect played by the process of sediment grading on bathymetry changes, not only because of the rate at which a waterway is silted up but also because of the character of the bed reconfiguration.

While performing the present calculations, the authors did not calibrate their model, in contrast to reported applications of the other models, whose results of computed morphological changes within a waterway are likewise presented in this article. It is not necessary to scale the present model because of the proposed method (that does not require scaling) of a mathematical description of sediment transport as well as bathymetry changes and interrelated changes in bed grain-size distribution, presented in greater detail by KACZMAREK et al. (2011) and SAWCZYŃSKI et al. (2011).

Recapitulating, the mathematical model presented in this paper can be recommended as a useful tool, which could be applicable to predicting bathymetry changes within hydroengineering constructions (waterways) and a rate of silting-up of navigation channels to harbours, but also to determination of grain-size distributions of sediments lying on the bed of a navigation channel.

Translated by JOLANTA IDŹKOWSKA

References

BIEGOWSKI J. 2006. *Graded seabed sediment dynamics: theory and experiment*. PhD thesis, IBW PAN Gdańsk.

BOSMAN J.J. 1982. *Concentration measurements under oscillating water motion*. Report on model investigation (M1965-II), Delft Hydraulics Laboratory.

BOSMAN J.J. 1985. *Concentration measurements in model and prototype*. Concept Delft Hydraulics Laboratory.

CHATELUS Y., KATOPODI I., DOHMEN-JANSSEN M., RIBBERINK J.S., SAMOTRAKIS P., CLOIN B.,SAVIOLI J.C., BOSBOOM J., O'CONNOR B.A., HEIN R., HAMM L. 1998. *Size Gradation Effects in Sediment Transport*. Proc. 26th ICCE, ASCE, Reston VA, p. 2435–2448.

HAVINGA F.J. 1992. *Sediment concentrations and sediment transport in case of irregular non-breaking waves with a current*. Delft Hydraulics Report H840.

KACZMAREK L.M. 1999. *Moveable Sea Bed Boundary Layer and Mechanics of Sediment Transport*. IBW PAN, Gdańsk.

KACZMAREK L.M., OSTROWSKI R. 2002. *Modelling intensive near-bed sand transport under wave-current flow versus laboratory and field data*. Coastal Engineering, 45(1): 1–18.

KACZMAREK L.M., BIEGOWSKI J., OSTROWSKI R. 2004. *Modelling cross-shore intensive sand transport and changes of grain size distribution versus field data*. Coastal Engineering, 51: 501–529.

KACZMAREK L.M., SAWCZYŃSKI Sz., BIEGOWSKI J. 2011. *Bathymetry changes and sand sorting during silting up of the channels*. Part 1. *Conservation of sediment mass*. Technical Sciences, 14(2): 153–170.

RIBBERINK J.S., AL-SALEM A. 1994. *Sediment transport in oscillatory boundary layers in cases of rippled beds and sheet flow*. Journal Geoph. Res., 99(C6): 12707–12727.

Rijn L.C. van 1985. *Flume experiments of sedimentation in channels by currents and waves*. Report S 347-II, Delft Hydraulics laboratory, Deflt, Netherlands.

Sánchez A., Wu W. 2011. *A Non-Equilibrium Sediment Transport Model for Coastal Inlets and Navigation Channels*. Journal of Coastal Research, 59: 39–48.

SANDPIT, Sand Transport and Morphology of Offshore Mining Pits. 2005. Eds. L.C. van Rijn, R.L. Soulsby, P. Hoekstra, A.G. Davies. Aqua Publications, The Netherlands, p. 716.

Sawczyński Sz., Kaczmarek L.M., Biegowski J. 2011. *Bathymetry changes and sand sorting during silting up of the channels*. Part 2. *Modelling versus laboratory data*. Technical Sciences, 14(2): 171–192.

Sistermans P.G.J. 2001. *Multi-fraction net sediment transports by irregular waves and a current*. Proc. Coastal Dynamics '01, ASCE, Reston VA, p. 918–927.

Walstra D.J.R., van Rijn L.C., Hoogewoning S.E., Aarninkhof S.G.J. 1999. *Modelling of sedimentation of dredged trenches and channels under the combined action of tidal currents and waves*. Coastal Sediment, 1999.

Walstra D.J.R., Chesher T., Davies A.G., Ribberink J., Sergent P., Silva P., Vittori G., Walther R., van Rijn L.C. 2005. *Intercomparison of the state of the morphological Models* [in:] *SANDPIT Sand Transport and Morphology of Offshore Mining Pits*. Eds. L.C. van Rijn, R.L. Soulsby, P. Hoekstra, A.G. Davies. Aqua Publications, The Netherlands.

THE EFFECT OF THE AGE OF SCOTS PINE (*PINUS SYLVESTRIS* L.) STANDS ON THE PHYSICAL PROPERTIES OF SEEDS AND THE OPERATING PARAMETERS OF CLEANING MACHINES

Zdzisław Kaliniewicz[1*], *Tadeusz Rawa*[1], *Paweł Tylek*[2], *Piotr Markowski*[1], *Andrzej Anders*[1], *Sławomir Fura*[3]

[1] Department of Heavy Duty Machines and Research Methodology
University of Warmia and Mazury
[2] Department of Mechanisation of Forest Works
University of Agriculture in Krakow
[3] Zdzisław Boroński Seed Extraction Plant in Ruciane Nida
Maskulińskie Forest Inspectorate

A b s t r a c t

Critical transport velocity, the thickness, width, length, the angle of sliding friction and weight of Scots pine seeds harvested from conservation seed stands were measured. Correlations were determined between the age of parent stands (124 to 180 years old) and the above parameters of Scots pine seeds. Significant correlations were found between the age of parents stands and the weight, dimensions and the angle of sliding friction of seeds. Such a correlation was not observed for critical transport velocity. The noted correlations were presented as first-order equations which show that among the studied seed properties, average seed weight changed to the highest degree – it decreased by ca. 15% as Scots pine trees grew older.

Symbols:
m – seed weight, mg,
S – standard deviation of property,
T, W, L – seeds thickness, width and length, mm,
w – age of parent trees, years
v – critical transport velocity of seed, $\mathrm{m \cdot s^{-1}}$,
V_s – coefficient of trait variability, %,
x – average value of property,
x_{max} – maximum value of property,
x_{min} – minimum value of property,
γ – angle of sliding friction of seed, °.

* Corespondence: Zdzisław Kaliniewicz, Katedra Maszyn Roboczych i Metodologii Badań, Uniwersytet Warmińsko-Mazurski, ul. Oczapowskiego 11/B112, 10-719 Olsztyn, tel. 89 523-39-34, e-mail: zdzisław.kaliniewicz@uwm.edu.pl

Introduction

The initial stage of tree growth is characterized by intensive development of vegetative organs. At the fruiting stage, more nutrient resources are invested into seeds, which slows down tree height growth. At a certain age, trees stop growing in height and the aging process begins. The life processes of trees weaken, and seeds become less plump. In Poland, Scots pines enter the old-growth stage at the age of ca. 100 years (MURAT 2002, PUCHNIARSKI 2008). In the present study, the following research hypothesis was formulated: seed weight and dimensions decrease as the tree stand grows older.

Harvested cones of Scots pine are extracted, and the produced seeds are dewinged. Dewinging supports the automation of further cleaning, storage, processing and sowing processes (MURAT 2005, PUCHNIARSKI 2008). Pine seeds are cleaned and sorted with the use of mesh sieves, pneumatic separators and machines that combine both functions (SARNOWSKA, WIĘSIK 1998). Separation processes rely on the following physical attributes of seeds: thickness, width and critical transport velocity. Analyses of selected physical properties of seeds from different seed lots (KALINIEWICZ et al. 2011) reveal significant differences. For this reason, the parameters of cleaning and sorting devices should be selected individually to account for the specific characteristics of a given seed stock. The above hypothesis has been validated by MURAT (2002) and SUSZKA et al. (2000). According to the cited authors, in order to preserve the genetic material, particular attention should be paid to separating the smallest seed fraction in the process of cleaning seeds from uneven-aged stands and from different trees of an even-aged stand, to prevent the removal of high-quality seeds together with small impurities (seed wings and wing fragments, husk fragments, dust) and empty seeds.

The aim of this study was to determine the effect of the age of old-growth parent Scots pine (*Pinus sylvestris* L.) stands on selected physical properties of seeds (critical transport velocity, the thickness, width, length, the angle of sliding friction and weight) and the operating parameters of cleaning machines.

Materials and Methods

The experimental material comprised Scots pine seeds harvested from cones collected in Seed Region 206 (Maskulińskie Forest Inspectorate, Regional Directorate of State Forests in Białystok, Poland) in 2009, from the following five old-growth conservation seed stands differing in age, with the following characteristics:

a) age – 124 years, forest site – Krzyże Forest Division 28/16/045, forest habitat – fresh forest, soil – rusty (marked as WDN-124),

b) age – 132 years, forest site – Guzianka Forest Division 28/16/045, forest habitat – fresh mixed forest, soil – rusty (marked as WDN-132),

c) age – 155 years, forest site – Borek Forest Division 28/16/045, forest habitat – fresh forest, soil – rusty (marked as WDN-155),

d) age – 162 years, forest site – Guzianka Forest Division 28/16/045, forest habitat – fresh mixed forest, soil – rusty podsol (marked as WDN-162),

e) age – 180 years, forest site – Borek Forest Division 28/16/045, forest habitat – fresh mixed forest, soil – rusty (marked as WDN-180).

Roughly 2 kg of pine cones were randomly selected from each batch of the harvested material supplied to the extraction plant in Ruciane Nida. Seeds were extracted by heating the cones five times in a stream of air (air temperature – ca. 60ºC, relative air humidity – ca. 40%, duration – 5 h) and cooling them at a low temperature (air temperature – –10ºC, relative air humidity – 80%, duration – 1 h). All seeds were removed from open cones by breaking off husks the wings of seeds were removed by rubbing in a linen bag. After impurities had been separated, the material was spread on a table and divided by halving (*Nasiennictwo...* 1995), to obtain samples of slightly more than 100 seeds each. The selected method produced samples of size: WDN-124 – 122, WDN-132 – 125, WDN-155 – 123, WDN-162 – 120, WDN-180 – 123. Such a sample size guaranteed standard errors of the mean smaller than 0.2 m · s⁻¹ for critical transport velocity, 0.1 mm for basic seed dimensions, 1º for the angle of sliding friction and 0.5 mg for seed weight. The relative moisture content of seeds in samples was similar, ranging from 7.6% to 8.3%.

At the first stage of the study, the critical transport velocity of seeds was determined using the Petkus K-293 pneumatic classifier within an accuracy of 0.11 m · s⁻¹ (measurement precision of air flow rate of 1 m3 · h⁻¹), according to the method proposed by KALINIEWICZ and TROJANOWSKI (2011).

Seed length and width were measured with the precision of 0.02 mm under an MWM 2325 workshop microscope, and seed thickness was determined with a dial indicator device, within an accuracy of 0.01 mm. The angle of sliding friction was determined on an inclined plane with an adjustable angle of inclination and a friction plate of ST3S steel (GPS – R_a = 0.46 µm), with the precision of 1º. The above measurements were performed as described by KALINIEWICZ et al. (2011).

The seeds were weighed on WAA 100/C/2 laboratory scales, within an accuracy of 0.1 mg.

At the second stage of the study, the separation of seeds with critical velocity below 5 m · s⁻¹ produced samples with the following number of Scots pine seeds: WDN-124 – 117, WDN-132 – 119, WDN-155 – 116, WDN-162 – 115, WDN-180 – 118.

The results were processed statistically using Statistica PL ver. 10 application, at a significance level of $\alpha = 0.05$, with the involvement of the following methods (LUSZNIEWICZ, SŁABY 2008):

– single classification analysis of variance – to compare the mean values of the attributes of Scots pine seeds from variously aged stands. When significant differences were observed, a post-hoc procedure with Duncan's test was employed to construct homogeneous subsets;

– correlation analysis – to determine correlations between the physical attributes of Scots pine seeds and the age of the parent stand, based on Pearson's linear correlation coefficients;

– linear regression – to determine a function describing the correlation between the age of the parent stand and selected physical attributes of seeds, based on the least squares method.

Results and Discussion

An analysis of the critical transport velocity of seeds (Fig. 1) revealed that each of the five distributions representing a different stand age had a bimodal character. Seeds with critical velocity below $5 \text{ m} \cdot \text{s}^{-1}$ were found to be empty in a slicing test. Seeds with higher values of critical velocity contained embryos at different stages of development. An analysis of seeds representing five stands (Tab. 1), divided into two fractions based on their critical transport velocity ($5 \text{ m} \cdot \text{s}^{-1}$), showed that they differed significantly also with respect to weight. No significant differences were noted between the dimensions (length, width and thickness) of seeds of the two fractions. According to reference data (GROCHOWICZ 1994), the critical transport velocity of seeds is determined, among others, by the ratio of their weight to cross-sectional area. Since empty and full Scots pine seeds do not differ significantly in dimensions (Tab. 1), there is a strong correlation between their critical transport velocity and weight. Thus, as observed also by TYLEK (1999), light impurities can be removed from the seed material using pneumatic separators, due to the absence of significant differences in seed dimensions and the fact that cleaning machines where seeds are separated based on weight are rarely used. It is important to set the proper air flow velocity because, according to SKRZYPCZYŃSKA and SKRZYSZEWSKI (2000), the percentages of empty seeds may differ considerably even in the material harvested in the same region. Another important consideration is the cost-effectiveness of seed pre-cleaning in a stream of air (SARNOWSKA, WIĘSIK 1998). This simple and efficient method is much cheaper that separation with the use of near-infrared radiation (850 to 2360 nm) and recording radiation that passes through or is reflected from

seeds (TIGABU, ODÉN 2003), which requires advanced and expensive equipment and is less effective.
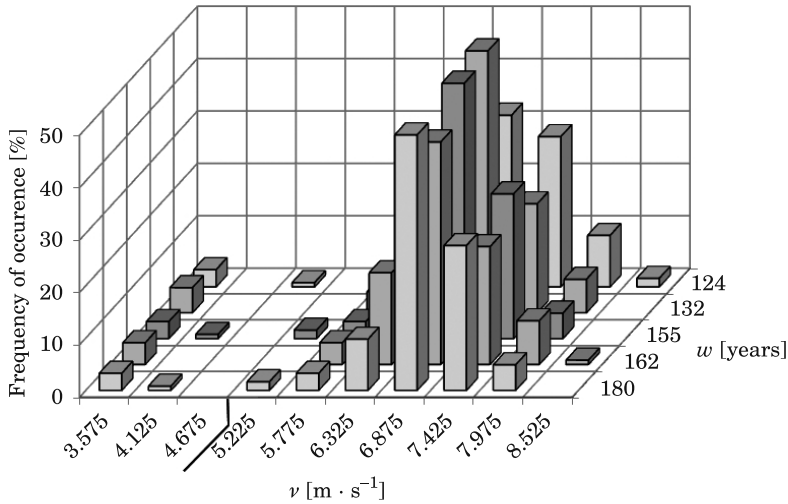

Fig. 1. Correlations between the critical transport velocity of seeds and the age of parent stands
Source: own study.

Table 1

A comparison of the average values of selected physical properties of seeds sorted based on critical transport velocity

Property	Limit of classification:	
	$v < 5 \text{ m} \cdot \text{s}^{-1}$	$v \geq 5 \text{ m} \cdot \text{s}^{-1}$
v	3.66^b	7.00^a
T	1.42^a	1.44^a
W	2.50^a	2.46^a
L	4.31^a	4.25^a
γ	35.4^a	30.0^b
m	2.04^b	5.89^a

[a, b] – different letters significant differences at the 0.05 level
Source: own calculations

Table 2 presents the statistical parameters of the physical attributes of seeds of different batches at the second stage of the experiment. The ranges of the dimensions and weight of Scots pine seeds collected from aging stands were as follows: thickness – from 0.99 to 1.89 mm, width – from 1.68 to 3.15 mm, length – from 3.30 to 5.28 mm, weight – from 3.4 to 10.4 mg. The above ranges are mostly consistent with those reported for selected tree stands in Poland (CZERNIK 1983, KALINIEWICZ et al. 2011, *Nasiennictwo...* 1995, TYLEK 1998)

Statistical distribution of the physical properties of seeds

Marking of stand	Property	x_{min}	x_{max}	x	S	V_s
WDN-124	v	5.78	8.53	7.03	0.594	8.45
	T	0.99	1.89	1.47	0.171	11.61
	W	2.06	3.19	2.49	0.227	9.09
	L	3.63	5.24	4.41	0.381	8.64
	γ	19	41	29.8	4.471	15.00
	m	3.6	10.4	6.36	1.579	24.83
WDN-132	v	5.78	7.98	6.97	0.471	6.76
	T	1.15	1.72	1.46	0.115	7.84
	W	2.10	3.07	2.56	0.197	7.71
	L	3.48	5.28	4.33	0.346	8.00
	γ	21	39	29.9	4.216	14.12
	m	3.6	9.0	6.24	1.144	18.33
WDN-155	v	5.23	8.53	7.07	0.600	8.48
	T	1.09	1.72	1.43	0.158	11.05
	W	2.01	2.97	2.48	0.179	7.21
	L	3.45	5.15	4.21	0.301	7.15
	γ	20	47	28.3	4.731	16.73
	m	3.4	8.7	5.83	0.956	16.40
WDN-162	v	5.78	8.53	6.97	0.550	7.89
	T	1.10	1.74	1.44	0.135	9.35
	W	1.68	2.79	2.40	0.189	7.89
	L	3.30	4.81	4.14	0.311	7.52
	γ	21	47	29.5	4.642	15.74
	m	3.5	8.8	5.58	1.078	19.33
WDN-180	v	5.23	7.98	6.97	0.510	7.32
	T	1.10	1.68	1.41	0.111	7.85
	W	2.02	2.93	2.41	0.163	6.76
	L	3.42	5.00	4.18	0.375	8.98
	γ	23	42	32.4	4.644	14.32
	m	3.4	7.3	5.45	0.857	15.73

Source: own calculations.

where the following values were noted: thickness – from 0.99 to 1.96 mm, width – from 1.72 to 3.18 mm, length – from 2.82 to 5.71 mm, thousand seed weight – from 4.0 to 9.8 g. The dimensions and weight of seeds are affected by the habitat and soil type, the genetic traits of tree stands, geographical location, weather conditions during cone and seed development, and even cone location in the tree crown (ANISZEWSKA 2006, BODYŁ et al. 2007, CASTRO 1999, KLUCZYŃSKI 1992, *Nasiennictwo*... 1995, OLEKSYN et al. 2001, SEVIK et al. 2010, SIVACIOĞLU 2010, SIVACIOĞLU, AYAN 2008, TURNA, GÜNEY 2009). An analysis of the significance of differences between the average values of the physical parameters of seeds harvested from variously aged stands (Fig. 2) indicated that the dimensions, weight and angle of sliding friction of seeds were also
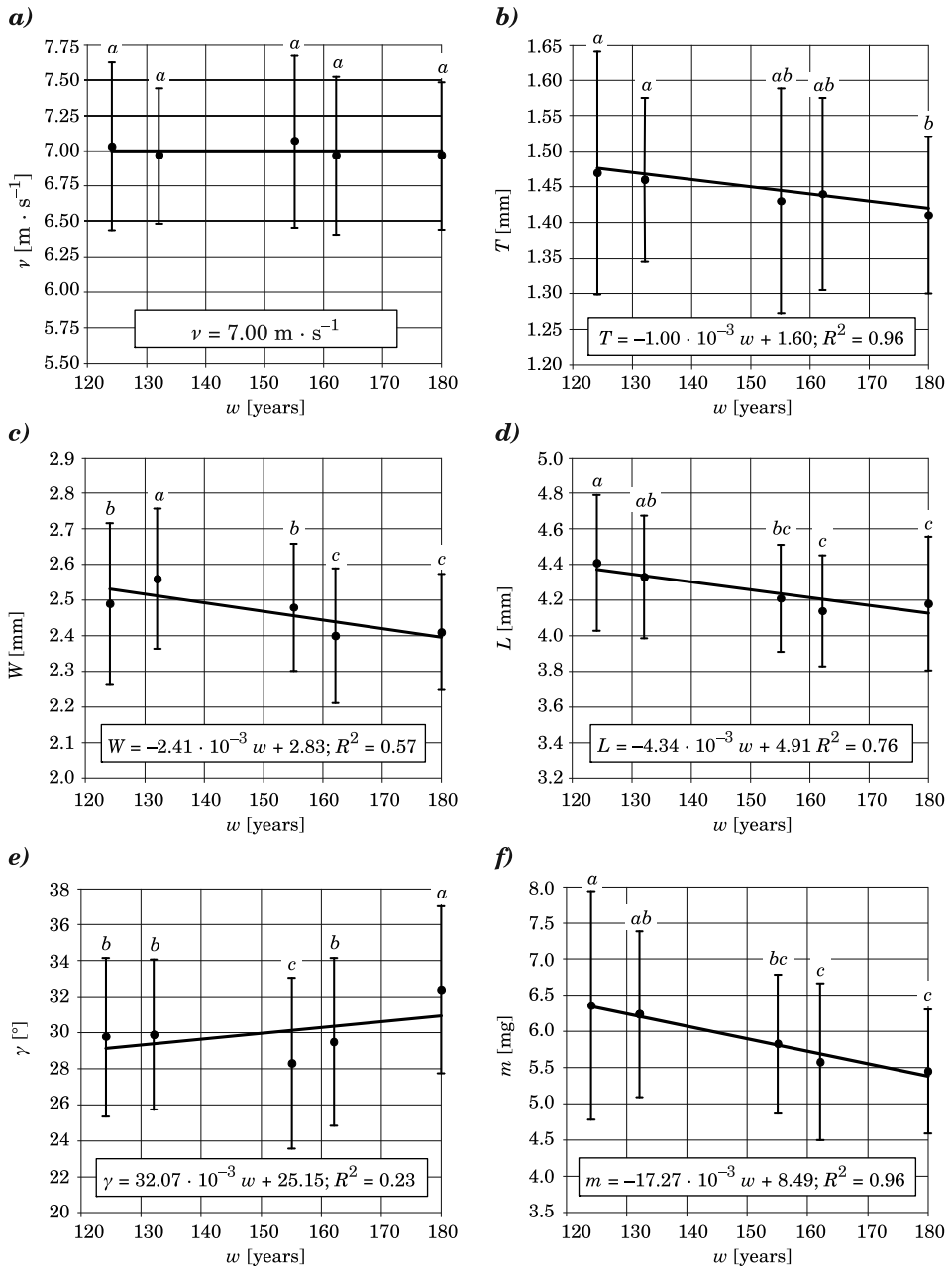
Fig. 2. The effect of the age of parent stands on the physical properties of Scots pine seeds: *a*) – critical transport velocity, *b*) – thickness, *c*) – width, *d*) – length, *e*) – angle of sliding friction, *f*) – weight; *a, b, c* – different letters denote significant differences at 0.05

Source: own study.

determined by the age of the parent stand. Statistically significant differences between seeds of different batches were not reported only with respect to the average values of critical transport velocity. It may be conclude that an increase in tree age is accompanied by a drop in the size and, consequently, the weight of seeds.

The coefficients of Pearson's linear correlation between the analyzed seed parameters (Tab. 3) showed that critical values were exceeded in 19 out of 21 cases. Correlations were not found between the age of the parent stand and the critical transport velocity of seeds, and between the angle of sliding friction and the length of seeds. The highest correlations were observed between the age of Scots pine stands and the weight, width and length of seeds. A strong correlation was also noted between the weight, critical transport velocity and dimensions of seeds. In the above cases, the values of correlation coefficients exceeded 0.5 and were considerably higher than the critical value of 0.08. Our results corroborate the findings of other authors regarding the seeds of Scots pine (BURACZYK 2010, CZERNIK 1983, SIVACIOĞLU 2010, TURNA, GÜNEY 2009) and other pine species (MATZIRIS 1997, SIVACIOĞLU, AYAN 2010).

Table 3

Coefficients of Pearson's linear correlation between the analyzed properties of seeds

Specification	w	v	T	W	L	γ	m
w	1	−0.019	−0.145	−0.245	−0.248	0.138	−0.293
v	–	1	0.597	0.285	0.121	−0.187	0.518
T	–	–	1	0.471	0.304	−0.239	0.727
W	–	–	–	1	0.444	−0.097	0.753
L	–	–	–	–	1	0.019	0.703
γ	–	–	–	–	–	1	−0.140
m	–	–	–	–	–	–	1

Critical value of the correlation coefficient at the 0.05 level – 0.081
Source: own calculations.

Equations describing the effect of the age of parent stands on selected physical attributes of Scots pine seeds are presented in Figure 2. The values of proportionality coefficients in the equations show that the weight and dimensions of seeds decreased, whereas the angle of sliding friction increased with the age of parent stands. The weight of seeds from a 180-year-old stand was by 15.2% lower than the weight of seeds from a stand aged 124 years, because the former are characterized by lower thickness, width and length – by 3.8, 5.3 and 5.6%, respectively.

Conclusions

1. The age of Scots pine parent stands (124 to 180 years) affected the weight, dimensions and the angle of sliding friction of seeds, but it had no influence on their critical transport velocity.

2. Seeds harvested from a 180-year-old stand were less plump that those collected from a stand aged 124 years; the differences in the average weight, length, width and thickness of seeds were ca. 15.2, 5.6, 5.3 and 3.8%, respectively. The range of changes in the dimensions of Scots pine seeds implies that the operating parameters of mesh sieves do not require adjustment.

3. Regardless of the age of old-growth stands, empty seeds can be separated from the seed material using pneumatic separators where the velocity of a vertical air stream in the aspiration channel reaches ca. 5 m · s⁻¹.

Translated by ALEKSANDRA POPRAWSKA

References

ANISZEWSKA M. 2006. *Connection between shape of pine (Pinus sylvestris) cones and weight, colour and number of seeds extracted from them*. Electronic Journal of Polish Agricultural Universities, Forestry, 9(1). Available online http://www.ejpau.media.pl/volume9/issue1/art-03.html.

BODYŁ M., WITOWSKA O., ZAŁĘSKI A. 2007. *Reasons for reduced viability of some Scots pine (Pinus sylvestris L.) seeds lots harvested in Poland in the winter season 2005/2006*. Leśne Prace Badawcze, 4: 47–65.

BURACZYK W. 2010. *Seed characteristics and morphological features of Scots pine (Pinus sylvestris L.) seedlings*. Leśne Prace Badawcze, 71(1): 13–20, doi:10.2478/v10111-009-0044-8.

CASTRO J. 1999. *Seed mass versus seedling performance in Scots pine: a maternally dependent trait*. New Phytol, 144: 153–161.

CZERNIK Z. 1983. *Studies of geometrical features of seeds of Scotch pine, Norway spruce and European larch*. Sylwan, 7: 31–40.

GROCHOWICZ J. 1994. *Maszyny do czyszczenia i sortowania*. Wyd. AR, Lublin.

KALINIEWICZ Z., GRABOWSKI A., LISZEWSKI A., FURA S. 2011. *Analysis of correlations between selected physical attributes of Scots pine seeds*. Technical Sciences, 14(1): 13–22.

KALINIEWICZ Z., TROJANOWSKI A. 2011. *Variability analysis and correlation of selected physical properties of black alder seeds*. Inżynieria Rolnicza, 8(133): 167–172.

KLUCZYŃSKI B. 1992. *Yielding and quality of Norway spruce (Picea abies (L.) Karst.) seeds in dependence on the part of crown and chosen biological and site-related characteristics of trees*. Sylwan, 5: 25–35.

LUSZNIEWICZ A., SŁABY T. 2008. *Statystyka z pakietem komputerowym STATISTICA PL. Teoria i zastosowanie*. Wyd. C.H. Beck, Warszawa.

MATZIRIS D. 1998. *Genetic variation in cone and seed characteristics in a clonal seed orchard of Aleppo pine grown in Greece*. Silvae Genet., 47(1): 37–41.

MURAT E. 2002. *Szczegółowa hodowla lasu*. Wyd. Oficyna Edytorska „Wydawnictwo Świat", Warszawa.

MURAT E. 2005. *Poradnik hodowcy lasu*. Wyd. Oficyna Edytorska „Wydawnictwo Świat", Warszawa.

Nasiennictwo leśnych drzew i krzewów iglastych. 1995. Red. A. Załęski. Wyd. Oficyna Edytorska „Wydawnictwo Świat", Warszawa.

OLEKSYN J., REICH P.B., TJOELKER M.G., CHALUPKA W. 2001. *Biogeographic differences in shoot elongation pattern among European Scots pine populations*. For. Ecol. Manag., 148: 207–220.

PUCHNIARSKI T.H. 2008. *Sosna zwyczajna hodowla i ochrona*. Wyd. PWRiL, Warszawa.

SARNOWSKA G., WIĘSIK J. 1998. *Wyłuszczarnia w Czarnej Białostockiej*. Część III. *Czyszczenie i separacja nasion*. Przegląd Techniki Rolniczej i Leśnej, 1: 19–21.

SEVIK H., AYAN S., TURNA I., YAHYAOGLU Z. 2010. *Genetic diversity among populations in Scotch pine (Pinus silvestris L.) seed stand of Western Black Sea Region in Turkey*. Afr. J. Biotechnol., 9(43): 7266–7272.

SIVACIOĞLU A. 2010. *Genetic variation in seed cone characteristics in a clonal seed orchard of Scots pine (Pinus sylvestris L.) grown in Kastamonu-Turkey*. Rom. Biotechnoll. Lett., 15(6): 5695–5701.

SIVACIOĞLU A., AYAN S. 2008. *Evaluation of seed production of scots pine (Pinus sylvestris L.) clonal seed orchard with cone analysis method*. Afr. J. Biotechnol., 7(24): 4393–4399.

SIVACIOĞLU A., AYAN S. 2010. *Variation in cone and seed characteristic in a clonal seed orchard of Anatolian black pine (Pinus nigra Arnold subsp. paliasiana (Lamb.) Holmboe)*. J. Environ. Biol., 31: 119–123.

SKRZYPCZYŃSKA M., SKRZYSZEWSKI J. 2000. *The qualitative estimation of Scots pine seeds originated from the selected localities of southern Poland*. Sylwan, 5: 85–90.

SUSZKA B., MULLER C., BONNET-MASIMBERT M. 2000. *Nasiona leśnych drzew liściastych od zbioru do siewu*. Wyd. Wydawnictwo Naukowe PWN, Warszawa-Poznań.

TIGABU M., ODÉN P.C. 2003. *Discrimination of viable and empty seeds of Pinus patula Schiebe & Deppe with near-infrared spectroscopy*. New Forests, 25: 163–176.

TURNA I., GÜNEY D. 2009. *Altitudinal variation of some morphological characters of Scots pine (Pinus sylvestris L.) in Turkey*. Afr. J. Biotechnol., 8(2): 202–208.

TYLEK P. 1998. *Cechy planimetryczne nasion drzew liściastych*. Przegląd Techniki Rolniczej i Leśnej, 1: 22–98.

TYLEK P. 1999. *Problems of pneumatic selection of forest tree seeds*. Sylwan, 12: 65–72.

PRACTICAL VERIFICATION OF THE PHONG REFLECTION MODEL CONDUCTED WITH THE USE OF TERRESTIAL LASER FIELD SCANING DATA

Kamil Kowalczyk[1], Jacek Rapiński[2], Dariusz Tomaszewski[2]*

[1] Chair of Land Surveying and Geomatics
[2] Institute of Geodesy
University of Warmia and Mazury in Olsztyn

A b s t r a c t

This paper is devoted to a practical verification of applying the Phong model, conducted based on available survey data obtained in field conditions. This model has already been described in previous articles, in which authors, using surveys performed in laboratory conditions, showed how to change the shape of the Phong model function depending on the material on which the laser beam falls. In subsequent publications, the focus was on the relationship between the incidence angle and the maximum distance that can be measured by the rangefinder. The measuring data were obtained as a result of scanning the furnace wall in the heat and power station in Pruszków, Poland with the use of reflectorless laser. The presented way of computation has been substantiated on the basis of calculated quantities, incidence angle and empirically defined parameters of the Phong model.

Introduction

Together with the technological advancements there appeared some new ways of taking observations that are successively being implemented into geodesy. In contemporary engineering surveys, reflectorless measurements are becoming more and more popular, allowing to shorten the time of obtaining stable results and increasing the number of data. These techniques have been fundamentally divided into two groups, Airborne Laser Scanning (ALS) which is based on placing the laser scanner on an airborne platform

* Corespondence: Jacek Rapiński, Instytut Geodezji, Uniwersytet Warmińsko-Mazurski, ul. M. Oczapowskiego 1, 10-719 Olsztyn, tel. 48 89 523-42-04, e-mail: jacek.rapinski@uwm.edu.pl

and Terrestrial Laser Scanning (TLS) where the device is placed on land surface.

The survey techniques mentioned above make use of a laser beam to determine the distance. An important issue then is a process of finding the farthest range which can be measured with the use of the given equipment. The main parameter considered for determining the maximum rangefinder range is the intensity. This quantity depends directly on the fraction of energy, which returns to the device after it is reflected off the object. There are numerous factors that affect the maximum measured range and the accuracy of taken observations. Intensity of a laser beam, however, depends directly on the atmospheric conditions, incidence angle, wave length, and the kind and color of substance from which the beam was reflected (KOWALCZYK, RAPIŃSKI 2011).

In the earlier publication (KOWALCZYK, RAPIŃSKI 2011) the authors introduced the theoretical Phong reflection model in laboratory conditions, proving the legitimacy of using it for modeling the maximum rangefinder range. The described model is mostly used in 3D computer graphics for determining some mirror reflections of imperfect objects. This model also allows for revealing the relations between the incidence angle of a laser ray and the partial energy that returns to the rangefinder.

The main objective of this paper is a practical verification of applying the Phong model, which will be conducted using available survey data, obtained in field conditions.

Registered energy and maximum rangefinder range

The measurements taken with TLS (scanners) can be considered in a similar way as those obtained by radars (SOUDARISSANANE et al. 2011). On the basis of this assumption, it is possible to derive a formula describing the amount of energy that returns to a rangefinder (1) (SABATINI, RICHARDSON 2010), later on referred to as the laser range equation:

$$P_R = \frac{\sigma D^4{}_{\mathrm{atm}}\ \tau_{\mathrm{sys}}\ P_T}{16 R^4\, \lambda K_a^2} \tag{1}$$

where:
P_R – recived Signal Power (Intensity),
P_T – tramsmitted Power (Intensity),
σ – effective target cross section,
K_a – aperture illumination constant,

R – range from system to target,
λ – wavelength,
D – aperture diameter,
τ_atm – atmospheric transmission factor,
τ_sys – system transmission factor.

While analyzing equation (1), one can observe that the influence on the total returned energy have factors that result from direct measurements conditions i.e. range from system to target, atmospheric transmission factor τatm and geometric conditions being the consequence of locating the device. The next crucial element for the initial intensity value is the construction of survey equipment, however, assuming that the same device is used, such effects values can be acknowledged as constant. A significant factor that affects the final result as well, is the effective target cross section σ, due to the fact that it is a quantity that describes the properties of a target (2) (VAIN et al. 2011).

$$\sigma = \pi\ \rho R^2 \beta_t^2 \cos\ \alpha \qquad (2)$$

ρ – reflectance of the target surface;
R – range from system to target;
β_t – beam width
α – incidence angle (angle between incoming laser beam and surface normal).

After applying some appropriate conversions and assuming that the whole beam has been reflected, the final formula for the range value is as follows (3):

$$R = \sqrt[4]{\frac{\rho D^2\ \tau_\text{atm}\ \tau_\text{sys}\ P_T}{8 P_R}} \qquad (3)$$

While taking measurements, the influence of the atmospheric conditions τ_atm has been omitted because the survey was conducted in a heat and power station, in which the temperature, humidity, etc. remained constant.

Theoretical Phong model

A fundamental model, specifically defined in physics, for determining the intensity of light reflected off the object, is the model developed by Lambert in 1760. Assuming that the model reveals a reflection from an ideal diffusely reflecting surface, the possibility of applying it in practice is restricted. Taking

into account a diversity of materials from which the objects, that the laser beam falls on, are made, one needs to apply some more advanced way of calculation. Due to the applied modifications, a theoretical Phong model constitutes an expansion of Lambert's idea, allowing to reflect the ray off secular surfaces. It is assumed that the returning beam of light satisfies the following equation (4) (ASHIKHMIN, SHIRLEY 2000):

$$I = I_i[k_d \cos \Theta + k_s \cos^n \Phi] \tag{4}$$

where:

I – the intensity of the reflected beam,
I_I – the intensity of the incidence beam,
k_d – the amount of beam that is diffused,
k_s – the amount of beam that is reflected,
Θ – incidence angle,
Φ – the angle between incidence angle and the viewer direction,
n – parameter describing the luminance of the material.

According to the Phong reflection model assumption, the final intensity value of the returning light, depends on the physical properties of the reflecting object, geometric measurement conditions and the incidence intensity value. The variables k_d, k_s and n are the quantities which make it possible to describe the influence that material has on the equation result. By correctly defining these parameters, it is possible to explicitly determine the influence of a reflecting surface type, color and structure (Fig. 1, 2, 3).
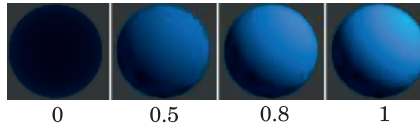

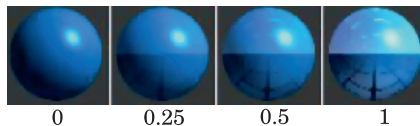Fig. 1. Sample values of k_d parameter varying according to reflecting material

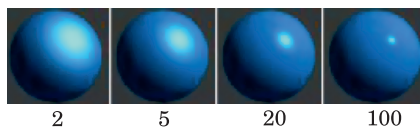Fig. 2. Sample values of k_s parameter varying according to reflecting material

Fig. 3. Sample values of n parameter varying according to reflecting material

The incidence angle and the angle between incidence angle and the viewer direction allow for taking into account the influence of the geometry of a falling laser beam. In case of a laser scanning the Φ angle is the same as the incidence angle. In Figure 4 shape of the considered function graph is shown in a polar coordinate system. In order to obtain such shape of the Phong model function the authors used as parameters values $n = 60$, $k_d = 0.2$ and $k_s = 0.8$.
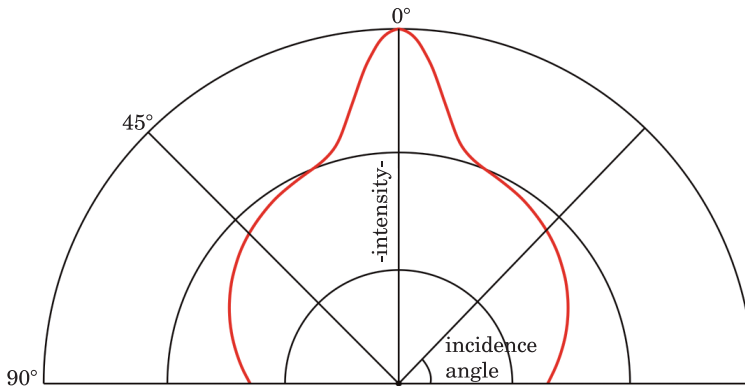

Fig. 4. Representation of the Phong function in a (polar) coordinate system

Testing the Phong reflection model in practice

As has already been stated in the introduction, this paper is devoted to the practical verification of the Phong model, conducted on the basis of field survey data. In order to perform this task, a set of points resulting from the laser scanning of the shield of a furnace in the heat and power station in Pruszków, Poland was used (Fig. 5).
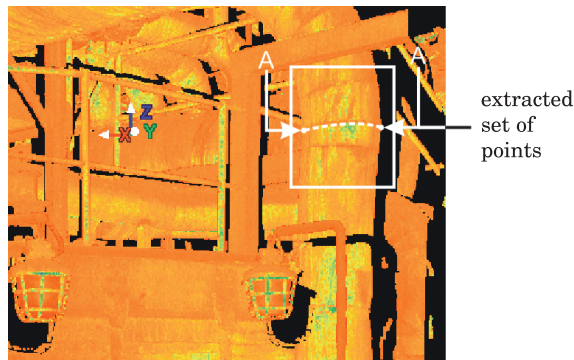

Fig. 5. Fragment of a point cloud representing the furnace in heat and power station

Result files from taken surveys contain coordinates (*X, Y, Z*) and intensity value for each point. In the cloud fragment presented above, one can see a heating pipe. Due to its cylindrical shape, a laser beam falling on such object, is reflected off different angles. This variability in incidence angle is considerably higher than in the case of flat surfaces. Making use of this property, a representative heating pipe had been chosen, from which, with the help of a surface perpendicular to the pipe direction, a set of points was extracted for later use (Fig. 6).
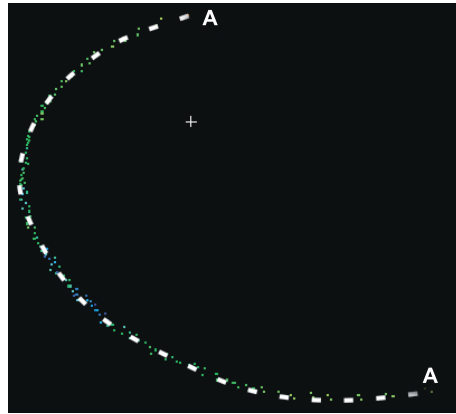

Fig. 6. Extracted set of points on a heating pipe

The next essential step for the Phong model realization was connected with finding the value of the incidence angle to each of the points. In order to achieve that, a curve was adjusted to the set of points. The root mean square error of the curve fit was equal 0.003436 m. Afterwards, normal and incidence angle were calculated for each of the points (Fig. 7). In such a way, all the quantities needed for performing the computation were collected.
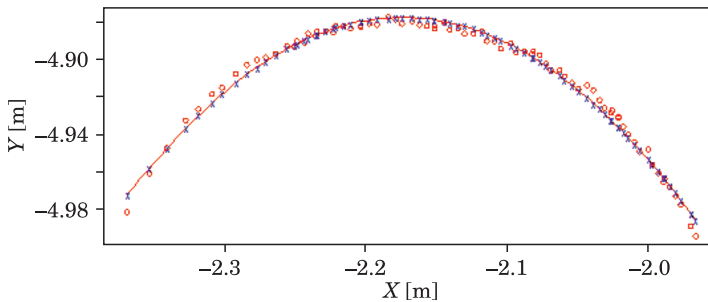

Fig. 7. A curve adjusted to a distinguished set of points

Results

The quantities, received as a result of the taken measurements and calculations, were used for drawing a suitable graph in the polar coordinate system. The way it was performed is analogous to the previous example (see Fig. 1). The task concerning the adjustment of the Phong model to the final function graph was carried out by an appropriate software. In this algorithm, the shape of the curve depended directly on the appropriate modification of the following parameters: k_d – the amount of beam that is diffused, k_s – the amount of beam that is reflected and n – luminance. The visualization of the Phong model function was graphically fitted to the extracted data set presented in the same polar coordinate system (Fig. 8). The variables were introduced based on physical properties of the substance from which the heating pipes had been made.
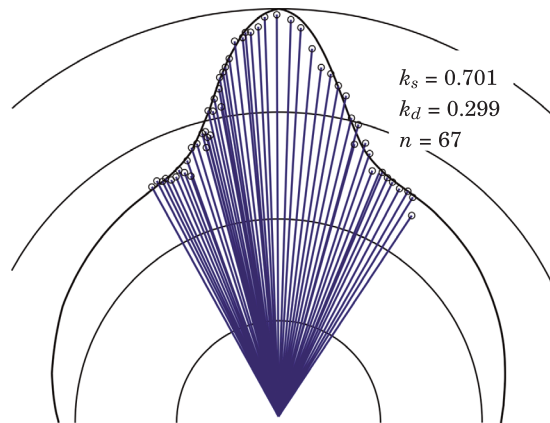

Fig. 8. Phong model adjusted to the measuring data

In the figure above, blue lines illustrate the survey data while a reflection curve is painted in black. The results clearly show that the Phong model can be used for reflectorless measurements. According to the findings obtained during some previous laboratory research (KOWALCZYK, RAPIŃSKI 2011), it can be concluded that in the case of matt substances, k_d – the amount of beam that is diffused, is considerably higher than k_s – the amount of beam that is reflected.

Conclusion

The results of the conducted research prove the legitimacy of the Phong reflection model used for picturing the intensity of returning a laser beam and maximum rangefinder range. The quantities obtained in the field conditions explicitly confirm the correctness of earlier laboratory research (KOWALCZYK, RAPIŃSKI 2011). This experimental way of determining the quantities k_s, k_d and n, for many substances, can later be used for establishing the physical properties of surfaces measured in terrain. Correct modeling of reflectorless surveys may constitute a new source of information taken into account while determining the border range measured by a given rangefinder.

Translated by DARIUSZ TOMASZEWSKI

Reference

ASHIKHMIN M., SHIRLEY P. 2000. *An Anisotropic Phong BRDF Model*. Journal of Graphics Tools, 5(2): 25–32.

RAPINSKI J., KOWALCZYK K. 2011. *The modelling of a reflectorless range finder maximum range with Phong model*. Reports on Geodesy. No.1 (90), Warszawa.

RAPINSKI J., KOWALCZYK K. 2011. *Verification of theoretical phong modelin reflectorless surveys*. Technical Sciences, 14(2): 255–261.

SABATINI R., RICHARDSON M.A. 2010. *RTO-AG-300-V26 Airborne Laser Systems Testing and Analysis*. NATO Research and Technology Organization.

SOUDARISSANANE S., LINDENBERGH R., MENENTI M., TEUNISSEN R. 2011. *Scanning geometry: Influencing factor on the quality of terrestrial laser scanning points*. ISPRS Journal of Photogrammetry and Remote Sensing, 66: 389–399.

VAIN A., LIBA N., SEPP K. 2011. *Factors affecting the airborne laser scanning intensity data*. Environmental Engineering, 3: 1511–1515.